공학석사학위논문

Position and Measurement Accuracy Analysis of GNSS Receiver using LQG based Vector Tracking Algorithm

LQG 기반 벡터 신호 추적 루프를 적용한 GNSS 수신기의 위치 및 측정치 정확도 분석

2017년 2월

서울대학교 대학원

기계항공공학부

박 민 혁

Abstract

Position and Measurement Accuracy Analysis of GNSS Receiver using LQG based Vector Tracking Algorithm

Minhuck Park

School of Mechanical and Aerospace Engineering

The Graduate School

Seoul National University

With the expansion of the navigation by GNSS, various studies have been conducted to improve the performance of navigation. From GNSS receiver's point of view, it can be possible to improve the performance of navigation by estimating more accurate position and measurements and developing more robust signal tracking loop in case of temporal signal block or decrement. To improve the accuracy of position and measurements, various studies based on estimation theory and control theory have been tried instead of using conventional loop filter. In this situation, through LQG theory, which combines optimal estimation theory, and optimal control theory, NCO inputs guarantee optimality under particular performance index. In addition, to improve the robustness of the signal tracking loop, vector tracking loop has been proposed. Eventually, by integrating LQG controller and vector tracking loop, LQG based vector tracking loop

has been proposed as signal tracking loop.

In this paper, simulation tool is developed to verify LQG based vector tracking loop in various conditions. First LQG based scalar tracking loop is designed to verify the performance of LQG controller. Measurements estimation errors in LQG based scalar tracking loop is smaller than those in LF based scalar tracking loop under various user’s dynamic.

Second LQG based vector tracking loop is designed. From the simple case, only pseudorange measurement and position state, simulation expands the complex case like pseudorange, carrier phase, and Doppler measurements and position, velocity, and clock bias state. As the number of satellites increase, the position and measurements estimation errors decrease. Also measurements estimation errors decrease compared to LQG based scalar tracking loop. Finally, in case of temporal signal power reduction, LQG based vector tracking loop is more robust than conventional signal tracking loop.

From this study, the performance of LQG based vector tracking loop is verified. Before applying LQG based vector tracking loop to GNSS receiver, performance analysis can be achieved rapidly using this simulation tool.

Keywords : Signal tracking, GNSS receiver, LQG control, Vector tracking loop, Scalar tracking loop, Position accuracy, Measurement accuracy

Student Number : 2015-20769

Contents

List of Figures

List of Tables

I. Introduction

1. Motivation and Objective

Currently, many users around the world are using navigation service through global navigation satellite system (GNSS). A user receives a signal broadcast from a time-synchronized satellites, calculates the distance between the satellite and the user, and calculates the user's position according to the triangulation method. GNSS applications are being applied not only for navigation of pedestrians, vehicles, ships, and aircraft, but also for various areas such as geodetic surveying, crustal deformation, and disaster detection.

The first and most popular GNSS is the global positioning system (GPS), which has been installed since 1995 in the United States. On a typical terrestrial user, the value of user equivalent range error (UERE) of the measurements provided by the GPS receiver is about 5.3m as the root mean square (RMS) value. The error factors are satellite orbit error, satellite clock error, ionospheric delay error, tropospheric delay error, and multipath error. The most significant error source is ionospheric delay error, about 4m. The position error is calculated by multiplying

the measurement error value by the dilution of precision (DOP), which is approximately 10m in error, depending on the satellite configuration [1].

In order to reduce the level of the position error, differential GPS (DGPS) that corrects the ionospheric delay error, satellite clock error, and satellite orbit error received from geostationary orbit (GEO) satellites has been studied. Also, real time kinematic GPS (RTK) method that calculates position using carrier phase has been studied [2]. Through the GPS modernization plan and GNSS signal modulation technique, the navigation performance has been improved [3, 4, 5].

Meanwhile from the GPS receiver's point of view, improving the internal algorithms has been done continuously. Most GPS receivers have been using signal tracking loop with loop filter since early days. Loop filter has been used steadily in the sense that simple to implement, has low computational load, and guarantees adequate performance.

However, in the 2000s as the result of the rapid development of the processor, the burden on the computational load has been reduced, and the signal tracking researches based on estimation and control theory have been studied. Especially, the signal tracking research based on linear-quadratic-Gaussian (LQG) generates optimal control input in certain performance index

through the Kalman filter and linear-quadratic regulator (LQR).

The conventional signal tracking loop is often used in a scalar tracking loop (STL), which estimates the measurements for each satellite and calculates the position based on the measurements. However, the STL is apt to lose the lock in the case of a temporal signal block or decrement. Even if the signal is restored, the receiver should be performed again from the acquisition process. To overcome this drawback, a vector tracking loop (VTL) has been proposed. The VTL collects measurements of each satellite, estimates the position first, and estimates measurements using estimated position. The difference of these algorithms makes it possible to design robust signal tracking loop. The above explanation is summarized as Figure I-1 below.

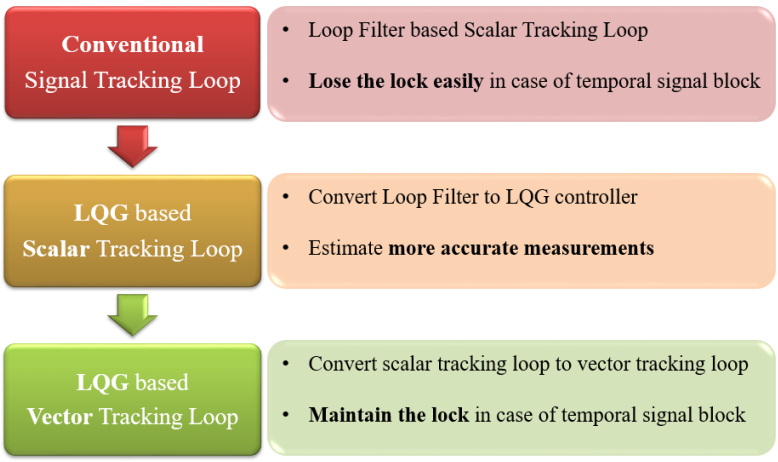

Figure I-1 Improvement of signal tracking performance

In this study, the performance analysis of LQG based vector tracking loop (LQG-VTL), combining VTL with LQG based signal tracking loop is conducted. Although LQG-VTL was studied in the past, only the performance verification through simulator data was carried out. Therefore, the performance analysis of LQG-VTL is performed under various conditions through simulation tool.

In order to verify the performance of LQG signal tracking loop, measurements estimation errors analysis of a LQG based scalar tracking loop (LQG-STL) versus a loop filter based scalar tracking loop (LF-STL) is carried out. Next, in order to verify the performance of LQG-VTL, measurements estimation error analysis against LQG-STL is performed and the position estimation error according to the number of satellites is analyzed. Finally, the analysis of measurements and position estimation error is performed in case of temporal signal power reduction.

2. Trends of Research

This paper shows that LQG-VTL is more accurate and robust than conventional LF-STL. First, the research, which develop conventional loop filter and replace the loop filter with

the LQG controller, will be described. Next, development trends for the VTL will be described. Finally, the research, which combine the LQG controller with VTL, will be described.

In order to improve the performance of conventional loop filter, the research which modify the loop filter and optimize equivalent noise bandwidth have been studied. Among the research which modify the loop filter, there is a FLL-assisted PLL scheme that performs signal tracking with the help of frequency locked loop (FLL) which tracks Doppler for carrier tracking through phase locked loop (PLL) [6, 7, 8]. Generally, the receiver controls the carrier phase through the FLL or the PLL. The FLL controls the error of carrier phase, otherwise the PLL controls the phase of carrier. The PLL can perform precise carrier phase tracking compared to the FLL, but is vulnerable to disturbance. This disadvantage can be compensated by the FLL-assisted PLL scheme.

The receiver can be robust to the user's dynamic environment but the noise becomes larger, as the bandwidth of the loop filter gets wider. However, when the bandwidth of loop filter is narrow, the receiver becomes vulnerable to the user's dynamic environment but the noise becomes small. Therefore, in the bandwidth of loop filter determines the performance of the tracking loop. The optimization of the equivalent noise bandwidth

has been studied [9].

So far, research on the improvement of the signal tracking based on the loop filter do not guarantee the optimality from the viewpoint of the control theory. However, since 2000, the development of processors has led to a variety of estimation theory based signal tracking research and control theory based signal tracking research. By combining the two, LQG based signal tracking loop can guarantee the optimal estimation and control input under particular performance index.

Jee proposed a method for LQG based signal tracking by applying the LQG controller to the Galileo BOC (1,1) signal [10]. In this paper, code and carrier tracking are performed through LQG controller and it is shown that the performance is improved compared to the conventional loop filter. Since the LQG algorithm proposed by Jee is modeled as a linear system, the signal tracking error can increase in a high dynamic environment. To overcome this problem, Im proposed a robust signal tracking loop in a high dynamic environment through unscented Kalman Filter and particle filter [11]. Jeon also proposed moving-set point LQG based signal tracking loop to converge cost function to 0 for every epoch [12]. The above three-research use the plant model proposed by Jee. However, the plant model proposed by Jee expresses the code error as the integral of Doppler value

when the control input term is not considered. It does not match the reality.

To overcome this drawback, Kim clarified the plant modeling [13]. The state of the LQG controller is the code delay, the carrier phase, and Doppler, and the control inputs are the deviation of the code numerically controlled oscillator (NCO) and the deviation of the carrier NCO. A realistic plant model, which propagates the code delay and the carrier phase as much as the integral of the Doppler value when the control input is zero, is proposed.

Research on the vector tracking loop began in 1980 with the aim of the integrating the signal tracking loop and navigation into one [14]. Spilker first used the term VTL in 1995, and proposed vector delay lock loop (VDLL) for code tracking [15]. The VTL has a disadvantage in that it has more computational load than conventional scalar tracking loop in which each signal tracking loop is performed independently. However, research on the VTL has been actively carried out by overcoming the problem of computation thanks to the development of technology in the 2000s.

Lashley proposed vector frequency locked loop (VFLL) as well as VDLL. In high dynamic and weak signal environment, he showed that the VTL is more robust than conventional scalar

tracking loop [16] [17] [18]. In addition, So proposed that near-far problem of pseudo-satellites is continuously estimated by the VTL [19], and Jeon proposed that the VTL can be applied to the low orbit satellite which is a strong dynamic environment [20].

A study of LQG based VTL (LQG-VTL) related to this study is [13] by Kim. Kim applied the VTL to the proposed LQG based signal tracking loop to improve the error of the NCO compared to the conventional VTL. However, the systematic performance analysis of LQG-VTL was not done in the above paper. In this paper, measurements and position estimation error of the LQG-VTL are measured systematically in various conditions through simulation tool.

3. Research Contents and Method

In this paper, I analyze the position and measurements performance analysis of LQG-VTL in various environments. The flow of this research is as follows.

Firstly, the reason why LQG-VTL is necessary is confirmed in terms the accuracy of position and measurements and robustness. Then I explain previous research to develop a signal tracking loop. Loop filter based research, LQG-STL research,

VTL research and finally LQG-VTL research are confirmed. Based on the above previous research, the performance analysis of LQG-VTL is carried out using simulation tool.

Secondly, the signal tracking loop is theoretically analyzed. I introduce the conventional LF-STL, LQG-STL, and LQG-VTL at the end. I explain the evolution process of the signal tracking loop and the characteristics of each signal tracking loop, thereby emphasizing the necessity of LQG-VTL.

Thirdly, I introduce simulation tool and simulation results for the performance analysis of position and measurements. Conditions of simulation tool and tuning method for LQG design are introduced. The performance analysis of measurements of LQG-STL is carried out compared to conventional LF-STL. After verifying the performance of the LQG-STL, the performance of the position and measurements of the LQG-VTL is verified by comparing that of the LQG-STL. Finally, in case of instantaneous signal power reduction, LQG-VTL is able to continuously maintain the lock compared to LF-STL.

4. Contribution

The model of the LQG based signal tracking loop used in this

study basically follows the model proposed by Kim [13]. Kim clearly set up a signal tracking loop that had been ambiguous in previous LQG based signal tracking loop studies [10, 11, 12]. Based on the proposed model, Kim designed the LQG controller to make LQG based signal tracking algorithm. Kim analyzed the performance of LQG-VTL based on simulator data. He conducted robustness tests on static user, low earth orbit satellite user in the situation of temporal signal reduction. The specific contribution of this research differentiated from [13] is as follows.

In this research, I develop a simulation tool for performance analysis of LQG-VTL. I simplified additional things besides the signal tracking loop and only compare the results from the signal tracking loop structure. It also makes it easy to add or change simulation conditions and enables simulations in various environments. Due to such simplification and ease of changing conditions, it can be possible to verify the performance evaluation in various conditions quickly.

The performance of LQG-VTL and LQG-STL is systematically analyzed using the simulation tool. First, in order to confirm the performance of LQG controller, the improvement of the measurements estimation errors of LQG-STL compared to LF-STL is confirmed. Through the above process, the

improvement of accuracy via the LQG controller is confirmed.

In the LQG-VTL simulation, a simulation is started from a simulation in which only pseudorange as measurement, and position as state of Kalman filter, which is the simplest condition. The simulation is expanded to complex case in which pseudorange, the Doppler, phase of the carrier as measurements, and the position, velocity, and clock bias as state of Kalman filter. Performance verification is confirmed by improving the measurements estimation errors compared to LQG-STL, and by improving the position and measurements estimation error in case a number of satellites increase. Finally, the tolerance of LQG-VTL is confirmed under the condition of temporal signal power reduction. In conclusion, improvement of robustness through VTL and improvement of accuracy by increasing number of satellites are verified.

Performance verification of LQG-VTL is carried out by improving measurements errors performance compared to LQG-STL and the position/measurements errors performance as the number of satellites increases. Finally, the tolerance of LQG-VTL is confirmed under the condition of signal power attenuation. In conclusion, we confirmed improvement of robustness through VTL and improvement of accuracy by increasing number of satellites.

II. Signal Tracking Loop of GNSS Receiver

In this chapter, the basic signal tracking loop of GNSS receiver is described briefly to understand the LQG based signal tracking covered in this paper. First, the structure of the GNSS signal and the principle of the GNSS receiver are described, and the loop filter based scalar tracking loop as typical signal tracking loop is introduced. Next, the principle and features of the vector tracking loop are described. In this research, it is done based on the GPS L1 C/A code, explanation is also described based on this.

1. Structure of GPS Signal

First, L1 C/A code signal is being broadcast from a GPS satellite can be expressed as Equation II-1.

$$s_{tmt}(t) = \sqrt{2P_{tmt}}\, D(t)x(t)\cos(2\pi f_{L1}t + \phi_{L1})$$

Equation II-1 Transmitted signal

In Equation II-1, $\sqrt{2P_{tmt}}$ represents signal power, $D(t)$ is navigation data, $x(t)$ is C/A code, and $\cos(2\pi f_{L1}t + \phi_{L1})$

represents carrier wave. P_{tmt} means the average transmission power, f_{L1} is the center frequency of the GPS L1 signal, and ϕ_{L1} is the phase of carrier wave. In other words, the transmitted signal from GPS satellite is calculated by the product of navigation data, C/A code, and carrier wave. It is shown in Figure II-1 [21].

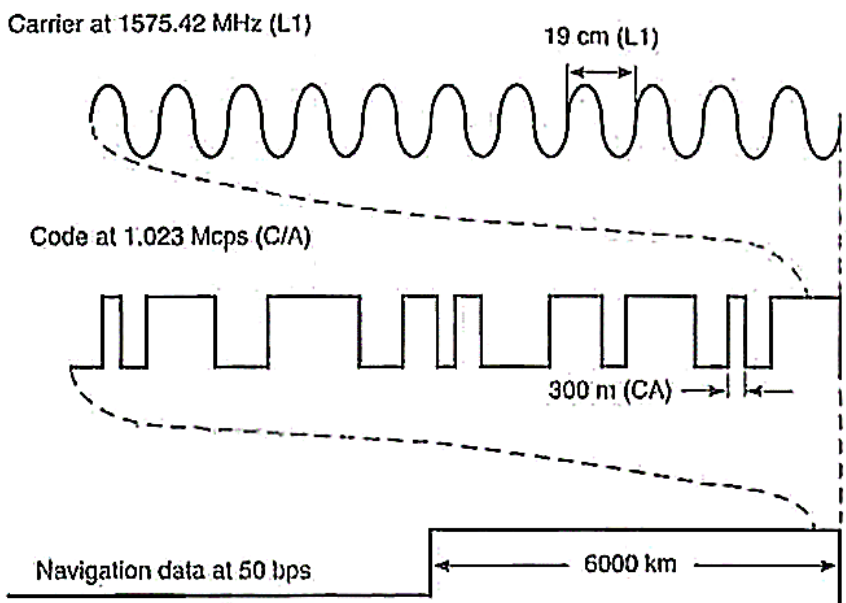

Figure II-1 GPS signal structure

The first figure in Figure II-1 means a carrier wave having a frequency of 1575.42 MHz and a wavelength of about 19 cm,

which corresponds to the L-band. The second figure in Figure II-1 means C/A code. The C/A code having a frequency of 1.023 Mcps is called PRN (Pseudo-Random Noise) code and is a unique identification code of 1023 binary type repeated every 1 ms. The autocorrelation of this PRN code has a value of 1. By designing the cross correlation with other satellites to be close to zero, the satellites can be identified. Also, the satellites can broadcast the signals to the same frequency by using feature of correlation. The difference between the phase of the received chip and the phase of the transmitted chip can know the distance and time information between the satellite and the user. The last part of Figure II-1 shows navigation data having a frequency of 50 bps and including information, which is necessary for operation in a binary format. The navigation messages include information such as satellite orbit information, satellite clock correction information, transmission time, etc. It takes at least 30 seconds to receive all data. In Figure II-2, the components of navigation data for each subframe are organized [22].

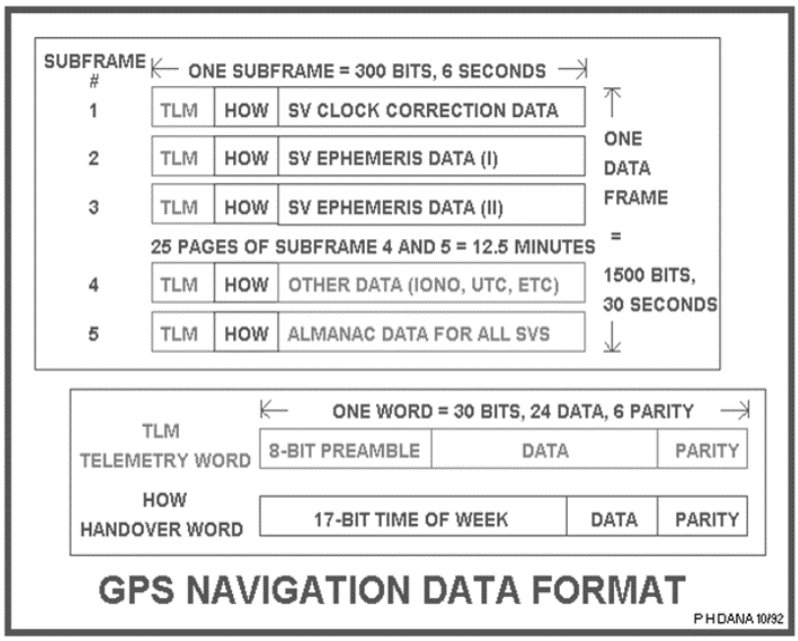

Figure II-2 GPS navigation data format

2. Structure and Principle of GPS Receiver

Figure II-3 shows a block diagram of a typical GNSS receiver [21].

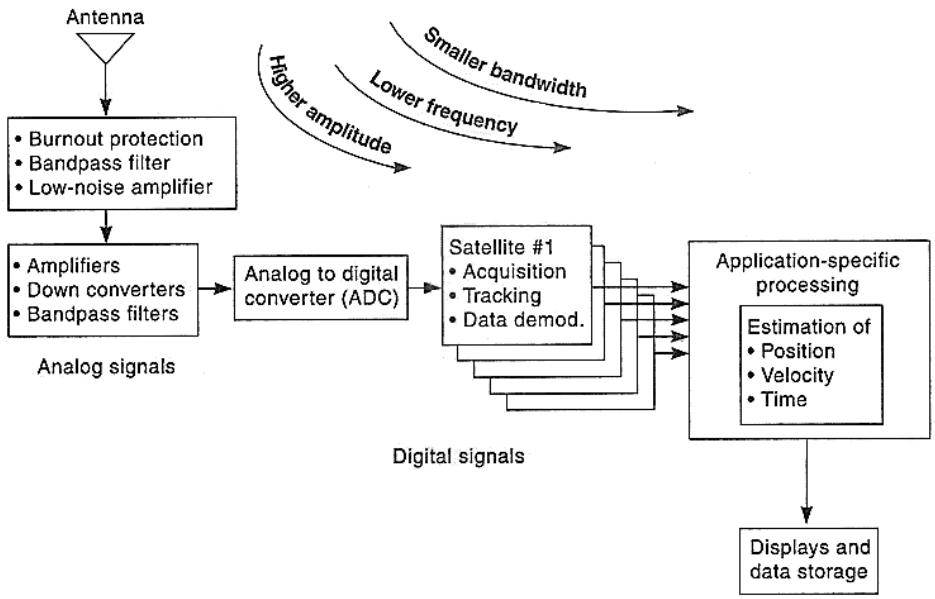

Figure II-3 Block diagram of typical GNSS receiver

The receiver receives the GNSS signal in the RF (Radio Frequency) state via the antenna, filters the signal with the bandwidth of interest via the bandpass filter, and lowers the noise level via lower-noise amplifier. Next, the signal of the center frequency of 1574.42 MHz is shifted to the IF (Intermediate Frequency) band by performing the down-converter and bandpass filter processing. By lowering the center frequency to the IF, it is possible to increase the efficiency of the bandpass filter, to alleviate the transmission of the noise in the RF band and the unexpected signal to baseband signal. The repetitive

process of down-converter and bandpass filter is called mixing, which is shown in the Figure II-4.

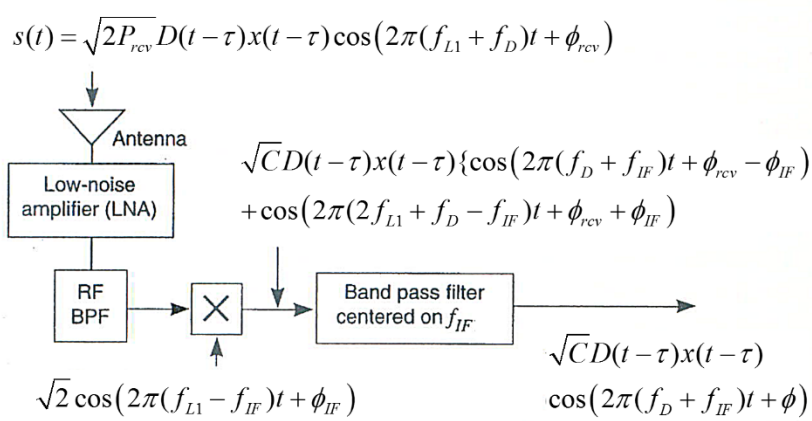

Figure II-4 Down-converter and band pass filter

According to Figure II-4, the satellite signal received at the antenna is expressed as Equation II-2.

$$s(t) = \sqrt{2P_{rcv}}D(t-\tau)x(t-\tau)\cos\left(2\pi(f_{L1}+f_D)t+\phi_{rcv}\right)$$

Equation II-2 Received Signal

Compared with Equation II-1, which is an equation of transmitted signal from the satellite, the power of signal is changed from $\sqrt{2P_{tmt}}$ to $\sqrt{2P_{rcv}}$, the navigation data and C/A

code are shifted by τ, the frequency of the carrier wave is shifted from f_{L1} to $(f_{L1}+f_D)$, and the phase of the carrier is shifted from ϕ_{L1} to ϕ_{rcv}. This is because the signal power is weakened, and the navigation data, distance between the satellite and the user, and the carrier phase are shifted as the signal has been transmitted. Also the frequency of carrier is changed by the Doppler effect depending on the speed of satellite and the user. The signal processed through the mixing process is expressed as follow.

$$s(t)=\sqrt{C}D(t-\tau)x(t-\tau)\cos\left(2\pi(f_{IF}+f_D)t+\varphi\right)$$

Equation II-3 Received signal after mixing process

It can be seen that the center frequency of the carrier is changed from f_{L1} to f_{IF} and $\phi_{rcv}-\phi_{IF}$ is represented by φ.

Up to the above process, the signal is an analog signal and is converted to a digital signal via ADC (Analog to Digital Converter). Before ADC processing, the signal is multiplied by a constant value via an AGC (Auto Gain Control) to increase the resolution of the signal. After AGC processing, the signal is converted into a digital signal according to sampling frequency

via a sampling process.

After converting the analog signal to the digital signal, the receiver calculates the user's position through signal acquisition, signal tracking, and data decoding process. The signal acquisition process is a process of searching for how many satellite signals are present in the received signal. At this time, the initial code delay value(τ) and Doppler value(f_D) can be found. The goal of the signal tracking process is to accurately estimate the code delay, the Doppler, and the carrier phase(φ) conclusively. By accurately estimating the above three values, it is possible to decode the navigation data and calculate the value of the measurements of the receiver such as the time sent from the satellites, pseudorange, Doppler, and carrier phase. Then using the above measured value, the receiver can calculate user's position.

3. Conventional Signal Tracking Loop

The goal of the signal tracking loop is accurately estimate the value of τ , f_D, and φ as described in the previous section. Within the receiver, a replica signal is generated using the

estimate value, and after measuring the error with the input signal, the estimated value is continuously corrected. Signal tracking loop is divided into DLL (Delay Locked Loop) in case of tracking τ, FLL (Frequency Locked Loop) in case of tracking f_D, and PLL (Phase Locked Loop) in case of tracking φ. In this research, the structure of the whole signal tracking loop is roughly explained in Figure II-5 without classifying three things separately.

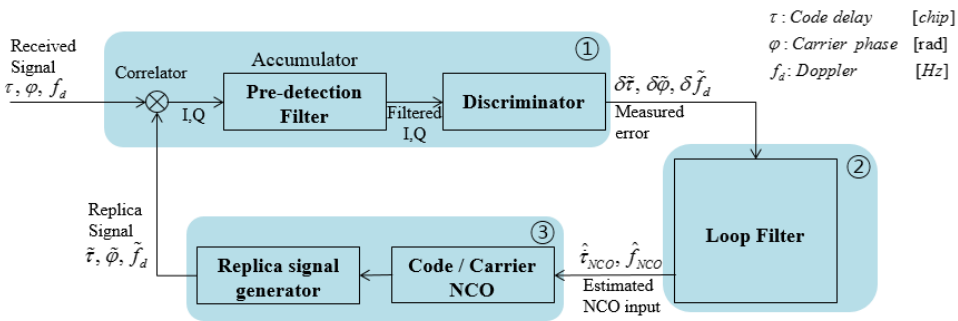

Figure II-5 Conventional signal tracking loop

(1) Discriminator

The part displayed in ① in Figure II-5 is the part that calculates the difference between received signal and replica signal. This part consists of a correlator, a pre-detection filter, and a discriminator. Their roles are as follows [6].

The correlator performs a mixing process of the received signal and the replica signal. At this time, cosine and sine are multiplied respectively in the signal, and these make In-phase (I) signal and Quadrature-phase (Q) signal.

The pre-detection filter is a part that executes coherent integration for a fixed integration time of the calculated I and Q. Through this process, the noise level of I and Q decreases. As the integration time increases, it is possible to receive a low C/N0 (Carrier-to-noise ratio) signal. But bit sync of navigation data should be performed priorly. In this paper, integration time is fixed in 1ms and the influence of pre-detection filter is not considered.

The discriminator calculates $\delta\tilde{\tau}, \delta\tilde{\varphi}, \delta\tilde{f}_D$, the tracking errors of τ, φ, f_D, through the filtered I and Q values. Each tracking error is calculated by taking one of several discriminator functions. Even though discriminator functions are nonlinear functions, they can be linearized approximately near zero. It is reasonable to approximate discriminator function linearly, since the error level is found in the linear area by the signal acquisition process.

Figure II-6 shows the code discriminator functions. In this study, 'Normalized Early Minus Late' discriminator is used.

Although this discriminator is large computation load, there is an advantage that linearity is excellent near zero. The equation of 'Normalized Early Minus Late' is as follows.

$$\delta\tilde{\tau} \approx \frac{1}{2}\frac{E-L}{E+L} \quad \left(E=\sqrt{I_E^2+Q_E^2}, L=\sqrt{I_L^2+Q_L^2}\right)$$

Equation II-4 'Normalized Early Minus Late'

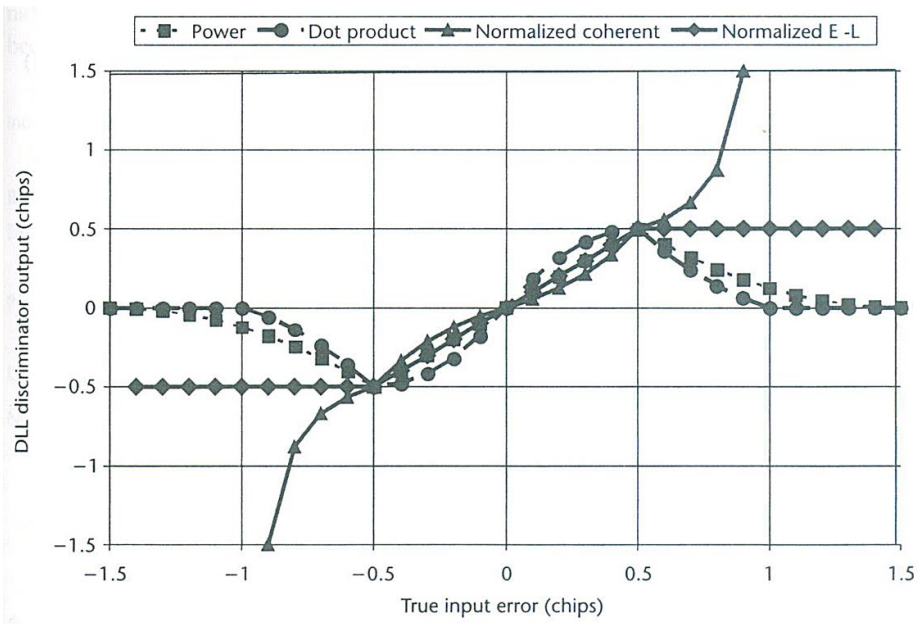

Figure II-6 Code discriminator functions

Figure II-7 shows the carrier discriminator functions. In this study, 'ATAN(Q/I)' discriminator is used. Although this

discriminator is large computation load, it shows good performance irrespective of the C/N0 value. The equation of 'ATAN(Q/I)' is as follows.

$$\delta\tilde{\phi} \approx ATAN(\mathrm{Q}/\mathrm{I})$$

Equation II-5 'ATAN(Q/I')

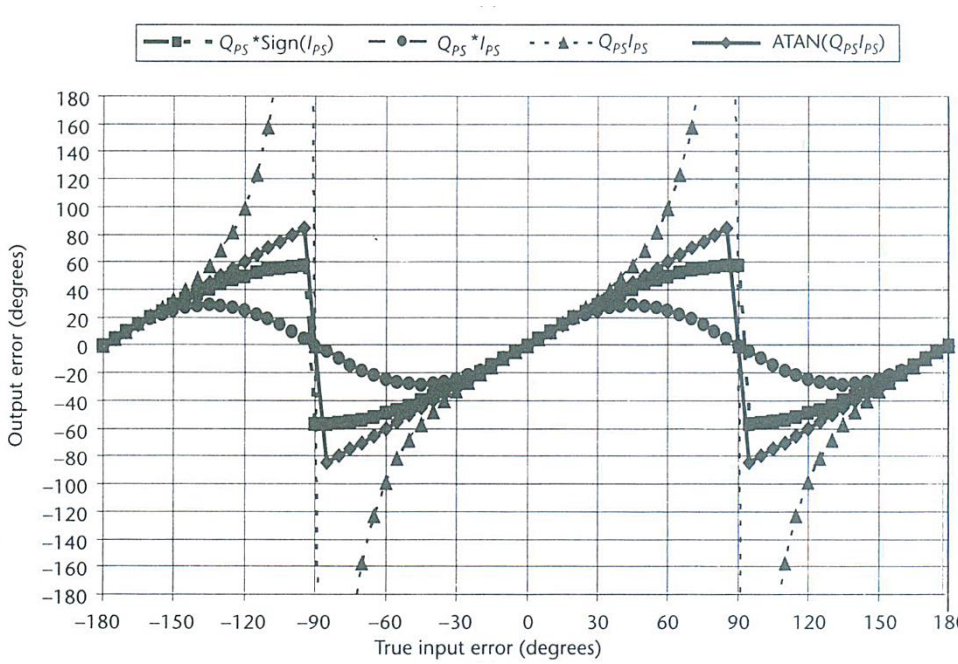

Figure II-7 Phase discriminator functions

Figure II-8 shows the frequency discriminator functions. In this study, 'sign(dot)(cross)' discriminator is used. This

discriminator shows good performance at a high C/N0, and has medium computation load. The equation of 'sign(dot)(cross)' is as follows.

$$\delta f_D \approx \frac{1}{2}\arcsin\left((cross)\times sign(dot)\right)$$

$$(dot = I_{k-1}\times I_k + Q_{k-1}\times Q_k \ , cross = I_{k-1}\times Q_k - I_k \times Q_{k-1})$$

Equation II-6 'sign(dot) (cross)'

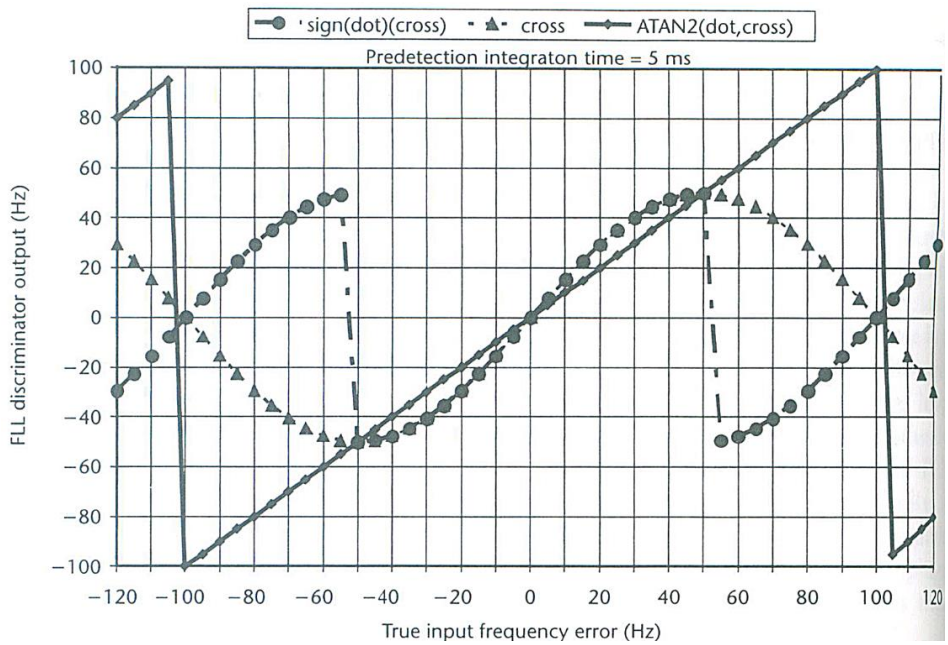

Figure II-8 Frequency discriminator functions

(2) Loop Filter

The part shown in ② of Figure II−5 is a loop filter that receives the error measured by the discriminator as an input and generates the NCO input. The characteristics of the loop filter are determined through the filter's order and the noise equivalent bandwidth. The larger the noise equivalent bandwidth, the faster the response speed, but the tracking accuracy of the signal is lower. The smaller the bandwidth, the higher the signal tracking accuracy, but the response speed is slower. Figure II−9 shows the block diagram according to the bandwidth of the loop filter. Table II−1 summarizes the values of coefficient according to the filter's order [6].

Loop Order	*Noise Bandwidth B_n (Hz)*	*Typical Filter Values*	*Steady State Error*	*Characteristics*
First	$\frac{\omega_0}{4}$	ω_0 $B_n = 0.25\,\omega_0$	$\frac{(dR/dt)}{\omega_0}$	Sensitive to velocity stress. Used in aided code loops and sometimes used in aided carrier loops. Unconditionally stable at all noise bandwidths.
Second	$\frac{\omega_0(1+a_2^2)}{4a_2}$	ω_0^2 $a_2\omega_0 = 1.414\omega_0$ $B_n = 0.53\,\omega_0$	$\frac{(d^2R/dt^2)}{\omega_0^2}$	Sensitive to acceleration stress. Used in aided and unaided carrier loops. Unconditionally stable at all noise bandwidths.
Third	$\frac{\omega_0(a_3b_3^2 + a_3^2 - b_3)}{4(a_3b_3 - 1)}$	ω_0^3 $a_3\omega_0^2 = 1.1\omega_0^2$ $b_3\omega_0 = 2.4\omega_0$ $B_n = 0.7845\,\omega_0$	$\frac{(d^3R/dt^3)}{\omega_0^3}$	Sensitive to jerk stress. Used in unaided carrier loops. Remains stable at $B_n \le 18$ Hz.

Table II−1 Loop filter characteristics

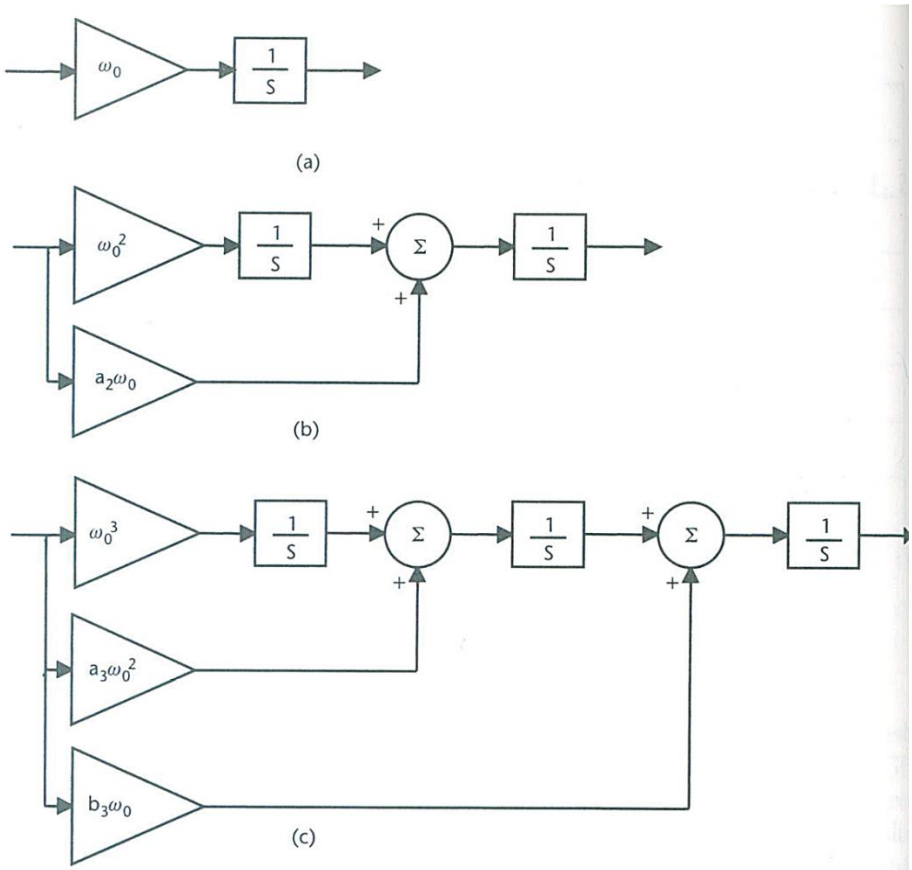

Figure II-9 Block diagrams of : (a) fist-, (b) second-, (c) third- order loop filters

The first order loop filter is vulnerable to the velocity input, the second order loop filter to the acceleration input, and the third order loop filter to the jerk input. In addition, when using the third order filter, stability should be considered. In the loop filter implemented in this paper for comparison to LQG controller, DLL

and FLL are used for the second order filter, and PLL is used third order filters, respectively.

(3) NCO

The part expressed by ③ in Figure II-5 generates a replica signal. The code NCO value and the carrier NCO generated by the loop filter are represented by $\hat{\dot{\tau}}_{NCO}$, $\hat{f}_{D,NCO}$ respectively. They become inputs to the NCO to generate a replica signal. The carrier NCO is Doppler estimate, the carrier estimate is the integral of the Doppler estimate, and the code estimate is the code NCO output integrated with the code NCO input.

4. Structure of Signal Tracking Loop

This section describes the structure of the scalar tracking loop (STL) and the vector tracking loop (VTL). The STL corresponds to the conventional signal tracking loop described in section 3. After describing the STL first, the structure and characteristics of the VTL is described by emphasizing the differences between STL and VTL.

(1) Structure of Scalar Tracking Loop

The structure of STL is shown in Figure II-10 [16].

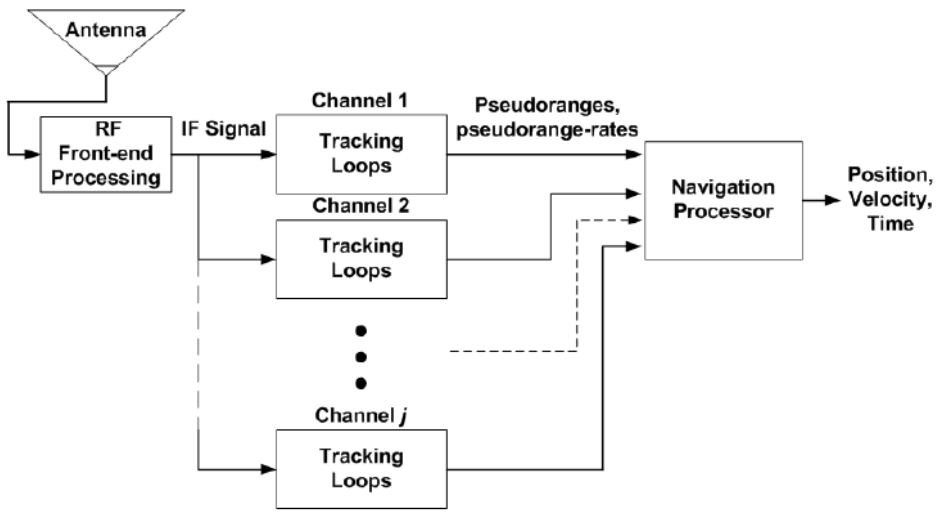

Figure II-10 Structure of scalar tracking loop

A signal tracking loop is performed for each channel, and in each signal tracking loop, measurements such as pseudorange and Doppler are calculated in parallel. The computed measurements in each channel are entered into the navigation filter, and the navigation solution is calculated. Figure II-10 shows that the process proceeds in one direction only. That is, the result of the navigation has no effect on the signal tracking

loop. However, the user's position and velocity, which are the navigation solution, actually have a direct correlation with the receiver's measurements. The signal tracking loop using this correlation is the VTL.

(2) Structure of Vector Tracking Loop

The structure of VTL is shown in Figure II-11.

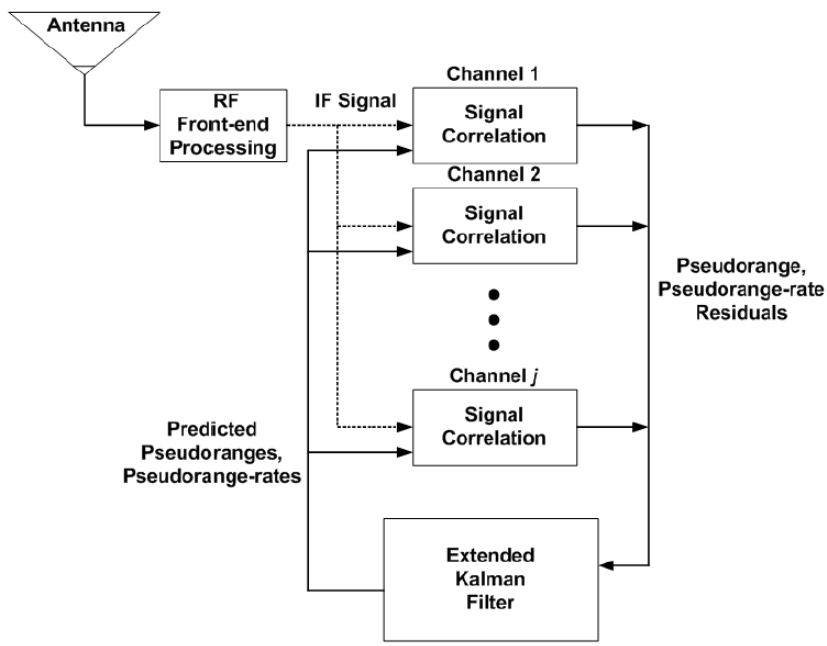

Figure II-11 Structure of vector tracking loop

Compared with Figure II-10, VTL operates with the

extended Kalman filter which is a navigation filter and estimates the measurements of each channel. The estimated measurements are used as input of the signal tracking loop again.

VTL has an advantage that it is more robust in the situation of signal interference than STL. Since the tracking loop estimate measurements at a time instead of being performed independently, the value of C/N0 of VTL that can tracks the signal is lower than that of STL. In addition, it is possible to estimate measurements for a temporal signal block or reduction situation through Kalman filter.

III. LQG based Signal Tracking Loop

In chapter 3, LQG based signal tracking loop is introduced. First, LQG control theory is divided into LQR controller and Kalman filter. Next, the structure of the LQG based scalar tracking loop (LQG-STL) used in this paper is introduced. Finally, the structure of LQG based vector tracking loop (LQG-VTL) is introduced.

1. LQG controller

Section 1 briefly looks at the LQG control theory based on the reference [23, 24, 25, 26, 27]. The LQG controller is a combination of the LQR controller based on the optimal control theory and the Kalman filter based on the optimal estimation theory. The LQG controller can be configured by combining two after designing each. First, the state equation of LQG controller can be expressed as Equation III-1.

$$x_{k+1} = Fx_k + Gu_k + \Gamma w_k \quad (w_k \sim N(0, W_d))$$

Equation III-1 State equation of LQG controller

In Equation III−1, k denotes an epoch, x_k denotes a state, u_k denotes an input, and w_k denotes process noise. The process for finding input u_k by LQR theory is as follows.

$$J = \min\left[\sum_{k=1}^{N} x_k{}^T Q x_k + u_k{}^T R u_k\right]$$
$$F^T P + PF - PGB^{-1}G^T P + A = 0$$
$$C = R^{-1}G^T P$$
$$u_k = -C\hat{x}_k$$

Equation III−2 Control gain of LQR controller

J is performance index function to generate a control input C for minimizing the value of J and C is calculated by finding P by algebraic Riccati equation (ARE) in the second row of Equation III−2. LQR tuning is done through adjustment of the weighting matrix A of the state, and the weighting matrix B of the input. The tuning of the weighting matrix will be explained in chapter 4.

Next, the method to estimate state variable based on Kalman filter theory is introduced. The estimation of the state x is the same as the following Equation III−3.

$$z_k = Hx_k + v_k \quad (v_k \sim N(0,R))$$

1. *Measurement Update*

$$\hat{x}_k = \hat{x}_k^- + K[z_k - Hx_k]$$

$$where\ K = P_k H^T R^{-1}$$

$$P_k^{-1} = M_k^{-1} + H^T R^{-1} H$$

2. *Time Update*

$$\hat{x}_{k+1}^- = F\hat{x}_k + Gu_k$$

$$M_{k+1} = FP_k F^T + \Gamma W_d \Gamma^T$$

Equation III-3 Kalman filter theory

The first expression of Equation III-3 is an equation about relationship between the state x_k and the measurement z_k. $\hat{x}_k^-$ and $\hat{x}_k$ are state variables before and after measurement update. P_k is the covariance matrix of $\hat{x}_k$, and M_k is the covariance matrix of $\hat{x}_k^-$. Tuning of the process noise covariance matrix W_d and measurement noise covariance matrix R is explained in chapter 4.

The above process is organized into a block diagram as shown in Figure III-1.

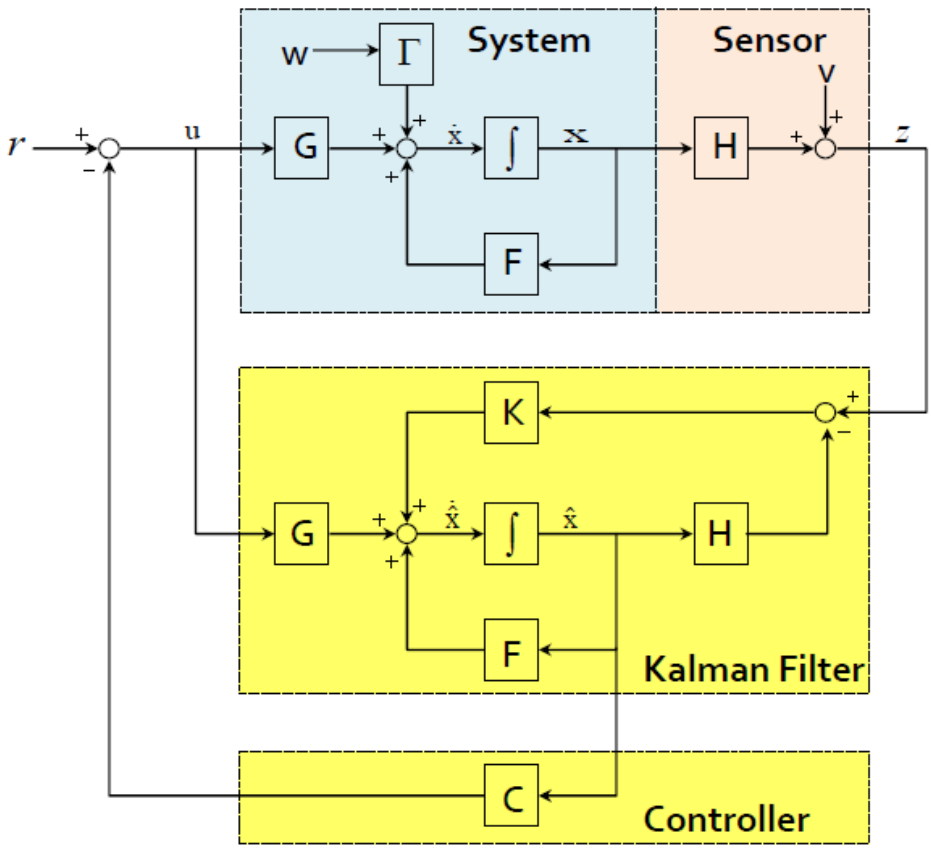

Figure III−1 Block diagram of LQG controller.

2. LQG based Scalar Tracking Loop

In this study, the loop filter is replaced with LQG controller in the signal tracking loop of the general GNSS receiver introduced in Figure II−5. As a result, an NCO input based on the

optimal control theory is generated, and improvement of measurement and position accuracy can be expected. The block diagram is shown in Figure III-2.

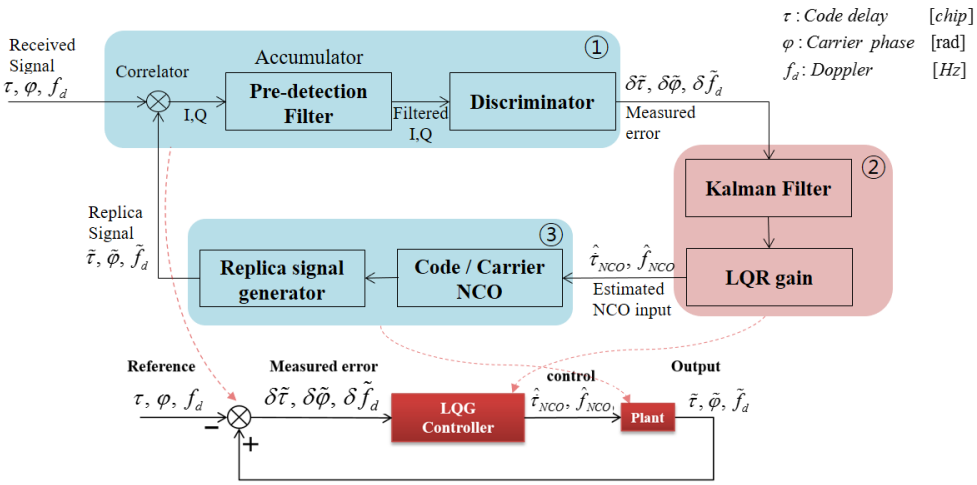

Figure III-2 LQG based scalar tracking loop (LQG-STL) (1)

Compared with Figure II-5, it can be confirmed that the part generating the NCO input is changed to the LQG controller. The block diagram at the bottom of **오류! 참조 원본을 찾을 수 없습니다.** is a revised version of that at the top. The discriminator part, ①, is ⊗ calculating error between received signal and replica signal. ② is LQG controller, and generating replica signal part, ③, is set to the plant. Figure III-2 is organized for each channel and re-expressed as shown in Figure III-3.

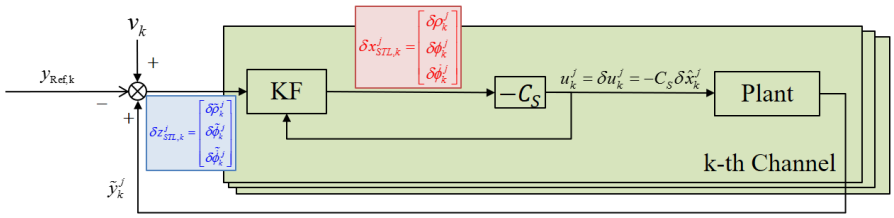

Figure III−3 LQG based scalar tracking loop (LQG−STL) (2)

Compared with Figure III−2, the measurement of the Kalman filter has changed from $\delta\tilde{\tau}_k^j$, $\delta\tilde{\varphi}_k^j$, $\delta\tilde{f}_{D,k}^j$ to $\delta\tilde{\rho}_k^j$, $\delta\tilde{\phi}_k^j$, $\delta\tilde{\dot{\phi}}_k^j$. This is done through unit conversion and is expressed in $\rho, \phi, \dot{\phi}$ instead of τ, φ, f_D for convenience of understanding. The unit conversion process is summarized as follows.

$$\tilde{\rho}_{k+1} = \tilde{\rho}_k + \Delta t\, \lambda_{\tilde{\tau}} \hat{\tilde{\tau}}_{NCO,k}$$
$$\tilde{\dot{\phi}}_{k+1} = \tilde{\dot{\phi}}_k + \lambda_f \hat{f}_{NCO,k}$$

ρ_k : *Pseudorange measurement* [m]
ϕ_k : *Carrierphase measurement* [m]
$\dot{\phi}_k$: *Doppler measurement* [m/s]
$\hat{\tilde{\tau}}_{NCO,k}$: *Code NCO* [$chip/\mathrm{sec}$]
$\hat{f}_{NCO,k}$: *Carrier NCO* [Hz]
$\lambda_{\tilde{\tau}}$: *Const converting units* (*chip to meter*)
λ_f : *Const converting units* (*Hz to m/s*)

Equation III−4 Unit conversion

In Figure III-3, the LQG controller is represented by the Kalman filter part and the control gain C_S of LQR controller. The measurements of the Kalman filter are discriminator errors (pseudorange, carrier phase, Doppler) for each channel. The state of the Kalman filter is also discriminator errors for each channel. The state equation and measurement equation of the Kalman filter are organized for k-th epoch, j-th channel as follows.

$$\delta x^j_{STL,k+1} = \begin{bmatrix} 1 & 0 & \Delta t \\ 0 & 1 & \Delta t \\ 0 & 0 & 1 \end{bmatrix} \delta x^j_{STL,k} + \begin{bmatrix} \Delta t & 0 \\ 0 & 0 \\ 0 & 1 \end{bmatrix} \delta u^j_k + w^j_{STL,k}$$
$$= F_{STL}\delta x^j_{STL,k} + G_{STL}\delta u^j_k + w^j_{STL,k}$$

Equation III-5 LQG-STL, Kalman filter state equation

$$\delta z^j_{STL,k} = \begin{bmatrix} 1 & 0 & 0 \\ 0 & 1 & 0 \\ 0 & 0 & 1 \end{bmatrix} \delta x^j_{STL,k} + v^j_k$$
$$= H_{STL}\delta x^j_{STL,k} + v^j_k$$

Equation III-6 LQG-STL, Kalman filter measurement equation

$$\delta x^j_{STL,k} = \begin{pmatrix} \delta\rho^j_k \\ \delta\phi^j_k \\ \delta\dot{\phi}^j_k \end{pmatrix} = \begin{pmatrix} \text{Code Tracking Error(m)} \\ \text{Carrier Phase Tracking Error(m/s)} \\ \text{Carrier Freq. Tracking Error(m)} \end{pmatrix}$$

$$\delta z^j_{STL,k} = \begin{pmatrix} \delta\tilde{\rho}^j_k \\ \delta\tilde{\phi}^j_k \\ \delta\tilde{\dot{\phi}}^j_k \end{pmatrix} = \begin{pmatrix} \text{Code Tracking Error(m)} \\ \text{Carrier Phase Tracking Error(m/s)} \\ \text{Carrier Freq. Tracking Error(m)} \end{pmatrix}$$

$$\delta u^j_k = \begin{pmatrix} \delta u^j{}_{\dot{\rho},k} \\ \delta u^j{}_{\dot{\phi},k} \end{pmatrix} = \begin{pmatrix} \delta\Delta\text{Code NCO} \\ \delta\Delta\text{Carrier NCO} \end{pmatrix}$$

Equation III-7 LQG STL, Definition of Kalman filter state, measurements and inputs

Next, passing the through the LQR controller, the input δu^j_k changes u^j_k via the detrim process adding $u^j_{k,0}(=u^j_k-\delta u^j_k)$. At this time, since u_0 is 0, it is finally $\delta u^j_k = u^j_k$. δx^j_k and δz^j_k are vector of (3×1) and δu^j_k is a vector of (2×1). Signal tracking is performed independently for each channel, and the plant equation is shown as follows.

$$x^j_{k+1} = \begin{bmatrix} 1 & 0 & \Delta t \\ 0 & 1 & \Delta t \\ 0 & 0 & 1 \end{bmatrix} x^j_k + \begin{bmatrix} \Delta t & 0 \\ 0 & 0 \\ 0 & 1 \end{bmatrix} u^j_k$$

$$\tilde{y}^j_k = \begin{bmatrix} 1 & 0 & 0 \\ 0 & 1 & 0 \\ 0 & 0 & 1 \end{bmatrix} x^j_k$$

Equation III-8 LQG-STL, Plant state equation

$$x_k^j = \begin{pmatrix} \rho_k^j \\ \phi_k^j \\ \dot{\phi}_k^j \end{pmatrix} = \begin{pmatrix} \text{Pseudorange (m)} \\ \text{Carrier Phase (m)} \\ \text{Doppler (m/s)} \end{pmatrix}$$

$$u_k^j = \begin{pmatrix} u_{\rho,k}^j \\ u_{\dot{\phi},k}^j \end{pmatrix} = \begin{pmatrix} \Delta\text{Code NCO (m/s)} \\ \Delta\text{Carrier NCO (m/s)} \end{pmatrix}$$

$$\tilde{y}_k^j = \begin{pmatrix} \tilde{\rho}_k^j \\ \tilde{\phi}_k^j \\ \tilde{\dot{\phi}}_k^j \end{pmatrix} = \begin{pmatrix} \text{Pseudorange (m)} \\ \text{Carrier Phase (m)} \\ \text{Doppler (m/s)} \end{pmatrix}$$

Equation III-9 LQG-STL, Definition of plant state

x_k^j and $\tilde{y}_k^j$ are a vector of (3×1), and u_k^j is a vector of (2×1).

3. LQG based Vector Tracking Loop

Next, LQG-VTL is introduced to improve the robustness of signal tracking. In Figure III-4, the block diagram of LQG-VTL is shown.

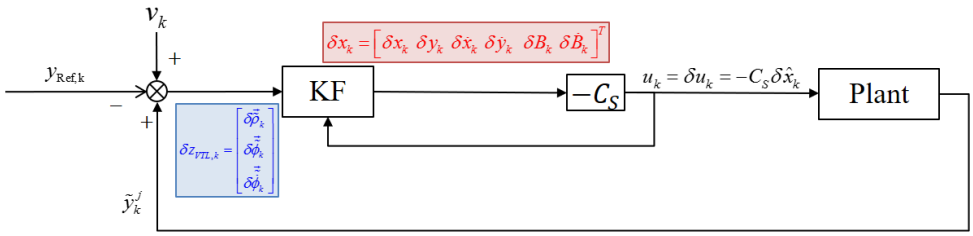

Figure III−4 LQG based vector tracking loop (LQG−VTL)

Compared with Figure III−3, it can be seen that the signal tracking loops for each channel are integrated into one. In addition, the measurements of the Kalman filter are expressed in the vector form in which measurements of all channels are collected, and the state of the Kalman filter is expressed in navigation solution. The state equation of the Kalman filter can be derived by the equation of scalar tracking loop. It is summarized together with measurement equation as follows.

$$\begin{aligned}\delta x_{VTL,k+1} &= \left(H_{w,k}^{\dagger} F_{STL} H_{w,k}\right)\delta x_{VTL,k} + \left(H_{w,k}^{\dagger} G_{STL}\right)\delta u_k + H_{w,k}^{\dagger} w_k \\ &= F_{VTL}\delta x_{VTL,k} + G_{VTL}\delta u_k + w_{VTL,k}\end{aligned}$$

Equation III−10 LQG−VTL, Kalman filter state equation

$$\delta z_k = -\begin{bmatrix} H_{m\times 2} & \bar{0}_{m\times 2} & -1 & 0 \\ H_{m\times 2} & \bar{0}_{m\times 2} & -1 & 0 \\ \bar{0}_{m\times 2} & H_{m\times 2} & 0 & -1 \end{bmatrix}\delta x_{VTL,k} + v_k = H_k \delta x_{VTL,k} + v_k$$

Equation III−11 LQG−VTL, Kalman filter measurement equation

$$\delta x_k = \begin{pmatrix} \delta Pos_k \\ \delta Vel_k \\ \delta B_k \\ \delta \dot{B}_k \end{pmatrix} = \begin{pmatrix} \text{Position Error (m)} \\ \text{Velocity Error (m/s)} \\ \text{Clock Bias Error (m)} \\ \text{Clock Drift Error (m/s)} \end{pmatrix}$$

$$\delta \vec{z}_{VTL,k} = \begin{pmatrix} \delta \vec{\rho}_k \\ \delta \vec{\phi}_k \\ \dot{\vec{\phi}}_k \end{pmatrix} = \begin{pmatrix} \text{Code Tracking Error (m)} \\ \text{Carrier Phase Tracking Error(m/s)} \\ \text{Carrier Freq. Tracking Error(m)} \end{pmatrix}$$

$$\delta \vec{u}_k = \begin{pmatrix} \delta \vec{u}_{\dot{\rho},k} \\ \delta \vec{u}_{\dot{\phi},k} \end{pmatrix} = \begin{pmatrix} \delta\Delta\text{Code NCO} \\ \delta\Delta\text{Carrier NCO} \end{pmatrix}$$

$$\begin{pmatrix} m \quad : \text{Number of } \textit{Satellites} \\ H_{m\times 2} : \textit{Line of Sight Matrix} \\ H_{w,k}^{\dagger} = (\mathrm{H}_k^T R^{-1} \mathrm{H}_k)^{-1} \mathrm{H}_k^T R^{-1} \end{pmatrix}$$

Equation III-12 LQG-VTL, Definition of Kalamn filter state, measurements

In the case of two-dimensional simulation, δx_k is a vector of (8×1), and $\delta \vec{z}_{VTL,k}$ is a vector of $(3m\times 1)$ when the number of satellites is m. Accordingly, $\delta \vec{u}_k$ is a vector of $(2m\times 1)$. $H_{m\times 2}$ constituting the H_k matrix is a line-of-sight vector for each satellite, and in the case of two-dimensional simulation, it is a matrix of $(m\times 2)$. $H_{w,k}$ is a value calculated via a weighted least square method and is necessary to reflect different values of C/N0 for each satellite. Next, the plant equation is as follows.

$$x_{k+1} = \begin{bmatrix} I_m & 0 & \Delta t \times I_m \\ 0 & I_m & \Delta t \times I_m \\ 0 & 0 & I_m \end{bmatrix} x_k + \begin{bmatrix} \Delta t \times I_m & 0 \\ 0 & 0 \\ 0 & I_m \end{bmatrix} u_k$$

$$\tilde{y}_k = \begin{bmatrix} I_m & 0 & 0 \\ 0 & I_m & 0 \\ 0 & 0 & I_m \end{bmatrix} x_k$$

Equation III-13 LQG-VTL, Plant state equation

$$x_k = \begin{pmatrix} \vec{\rho}_k \\ \vec{\phi}_k \\ \dot{\vec{\phi}}_k \end{pmatrix} = \begin{pmatrix} \text{Pseudorange (m)} \\ \text{Carrier Phase (m)} \\ \text{Doppler (m/s)} \end{pmatrix}$$

$$u_k = \begin{pmatrix} \vec{u}_{\dot{\rho},k} \\ \vec{u}_{\dot{\phi},k} \end{pmatrix} = \begin{pmatrix} \Delta\text{Code NCO (m/s)} \\ \Delta\text{Carrier NCO (m/s)} \end{pmatrix}$$

$$\tilde{y}_k = \begin{pmatrix} \tilde{\vec{\rho}}_k \\ \tilde{\vec{\phi}}_k \\ \tilde{\dot{\vec{\phi}}}_k \end{pmatrix} = \begin{pmatrix} \text{Pseudorange (m)} \\ \text{Carrier Phase (m)} \\ \text{Doppler (m/s)} \end{pmatrix}$$

Equation III-14 LQG-VTL, Definition of plant state

x_k and $\tilde{y}_k$ are the vector of $(3m \times 1)$, and $\delta\vec{u}_k$ is a vector of $(2m \times 1)$. I_m is the m-th identity matrix. The process of the LQG-VTL represented in Figure III-4 is described in detail as follows.

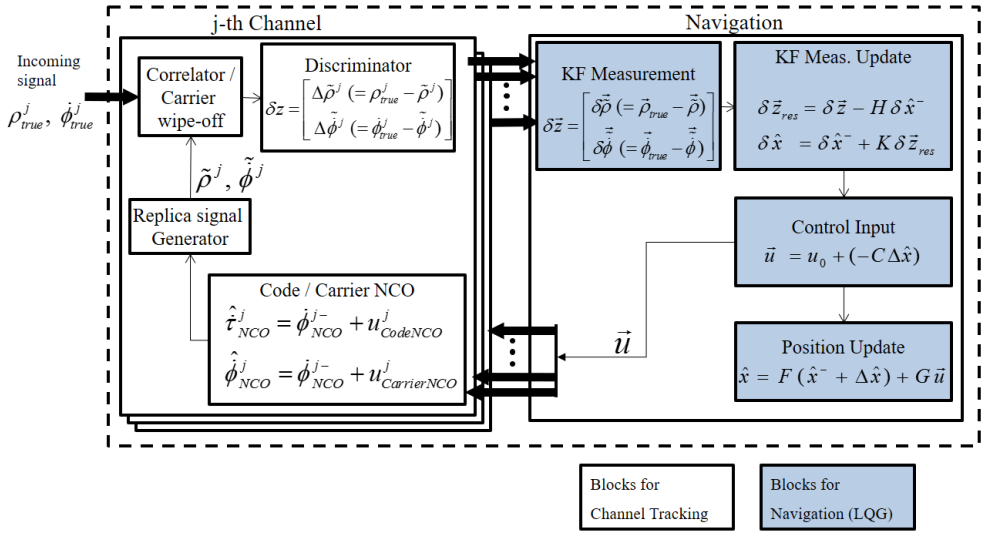

Figure III-5 Structure of LQG-VTL

Figure III-5 shows the structure of VTL implemented in this paper in more detail. The discriminator calculates the difference between the received signal and replica signal generated by the replica generator. The outputs of discriminator for each channel are the measurements of the Kalman filter. The LQG controller then generates the control input and updates the navigation solution and the state of the Kalman filter. The generated control inputs are divided into the NCO of each channel to update the NCO input, thereby generating the replica signal.

IV. Simulation Environment and Results

In chapter 4, the simulation tool implemented to investigate the performance of LQG-VTL described in chapter 3 is explained. The objective, and implementing method of the simulation tool and tuning method of the LQG controller used for the simulation are introduced. Then, the order of the simulation and the results associated with it are introduced.

1. Simulation Tool

(1) Objective and Method

In this paper, LQG-VTL is verified by using the developed simulation tool. The evaluation is performed by dividing the theoretically established LQG based signal tracking loop into STL and VTL and showing the performance improvement instead of conventional signal tracking loop. LQG-STL is verified by showing that measurement accuracy is improved compared to the conventional LF-STL. LQG-VTL shows improved measurement accuracy compared with LQG-STL. Also, position and measurements errors of VTL decrease when the number of

satellites increases.

Starting from the simplest environment, this simulation tool verifies performance one by one while adding conditions one by one. Implementation of the simulation tool is based on two dimensions, and the two-dimensional axis is defined as Figure IV-1.

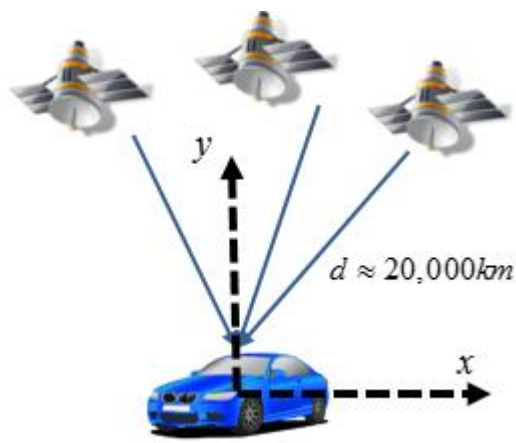

Figure IV-1 Coordinate of 2D simulation

For simulation, the true position and velocity of user and satellites is set, thereby generating the true measurements, pseudorange, carrier phase, and Doppler. The input variable of the simulation tool and the options that can be selected are as follows.

Input variable	option
Dimension	2D / 3D
Measurements	(ρ) / (ρ, $\dot{\phi}$) / (ρ, ϕ, $\dot{\phi}$)
State	(ρ, ϕ, $\dot{\phi}$) – STL (Pos) / (Pos,Vel) / (Pos,Vel,B,$\dot{B}$) – VTL
User's dynamic	Static / Circular / Const.Vel / Const.Accel
Satellites dynamic	Static / Circular
C/N0	30dB*Hz ~ 45dB*Hz
Disturbance	No consideration / Consideration

Table IV-1 Input variable of simulation tool

In the results introduced in this paper, the satellites are fixed, and various error factors (ex. ionosphere, troposphere delay error) are not considered. Simulation is performed in a simple environment, but there is no problem to judge the performance of the signal tracking loop.

(2) LQR Controller Tuning

In order to design the LQG controller, it is necessary to set the weighting matrix of the LQR controller, the process noise covariance matrix, and the measurement noise covariance matrix

of the Kalman filter.

The design of the LQR controller is determined by Bryson's rule and its method is as follows.

$$A_{ii} = \frac{1}{\text{maximum acceptable value of } x_i^2}, i \in \{1, 2, ..., \text{number of states}\}$$

$$B_{jj} = \frac{1}{\text{maximum acceptable value of } u_j^2}, j \in \{1, 2, ..., \text{number of controls}\}$$

Equation IV-1 Bryson's rule

A is the weighting matrix of the state, and B is the weighting matrix of the input. Weighting is set to the reciprocal of the square of the possible maximum value. As the maximum possible value is larger, the weighting is set smaller and the influence on the performance index can be reduced. The LQR tuning values implemented in the LQG-VTL and LQG-STL in this paper are as follows.

LQG-STL	$A = diag\left(\frac{1}{\rho_{\max}^2}, \frac{1}{\phi_{\max}^2}, \frac{1}{\dot{\phi}_{\max}^2}\right) = diag\left(\frac{1}{1^2}, \frac{1}{0.001^2}, \frac{1}{0.09^2}\right)$ $B = diag\left(\frac{1}{u_{\rho,\max}^2}, \frac{1}{u_{\dot{\phi},\max}^2}\right) = diag\left(\frac{1}{150^2}, \frac{1}{1/20^2}\right)$

LQG-VTL	$A = diag(\frac{1}{x_{\max}^2}, \frac{1}{y_{\max}^2}, \frac{1}{\dot{x}_{\max}^2}, \frac{1}{\dot{y}_{\max}^2}, \frac{1}{B_{\max}^2}, \frac{1}{\dot{B}_{\max}^2})$ $= diag(\frac{1}{1^2}, \frac{1}{1^2}, \frac{1}{100^2}, \frac{1}{100^2}, \frac{1}{1^2}, \frac{1}{100^2})$ $B = diag\left(\frac{1}{u_{\rho,\max}^2}, \frac{1}{u_{\dot{\phi},\max}^2} \right)$ $= diag\left(\frac{1}{150^2}, \frac{1}{1/20^2} \right)$

Table IV−2 LQR weighting matrix tuning

The weighting matrix of the state is set to the degree of the desired error level and the weighting matrix of the input is set with the maximum error value that can occur in the course of signal acquisition process. In the course of signal acquisition, a maximum error of pseudorange is 0.5 chips, which is 150 m when converted to distance. In Doppler, when acquiring signals at intervals of up to 500 Hz, a maximum error of Doppler is up to 250Hz, which is 50 m/s when converted to speed. To converge 150 m and 50 m/s within 1 second, the maximum value of each input shall have values of 150 m and 1/20 m/s.

(3) Kalman Filter Tuning

The measurement noise covariance matrix R can be

calculated based on the value of C/N0 in the process of converting the output value of the discriminator to I and Q. In this simulation, R is determined based on each C/N0. For example, the measurement noise covariance matrix at 45 dB*Hz is as follows. In Equation IV-2, the components of R in turn mean the noise level of the pseudorange, carrier phase, and Doppler.

$$R = diag\left(25^2 \;\; 0.004^2 \;\; 6^2\right)$$

Equation IV-2 Measurement noise covariance matrix (45dB*Hz)

The setting method of process noise covariance matrix W_d of the Kalman filter is introduced in various ways in following reference papers [27] [28] [29] [30] [31]. In this paper, the W_d is set by using a new method.

Rewriting the time update equation and the measurement update equation of the Kalman filter introduced in Equation III-3 is as follows.

$$P_k^{-1} = M_k^{-1} + H^T R^{-1} H$$
$$M_{k+1} = F P_k F^T + \Gamma W_d \Gamma^T$$

Equation IV-3 Kalman filter measurement update / time update

P is the covariance matrix of the error of the state, which means the desired error level of state. That is, after setting P matrix first, W_d is calculated in reverse. Define the desired error covariance matrix of the state as C. In the steady state, k−th epoch and k+1−th epoch are same, $P_k \approx P_{k+1}$, $M_k = M_{k+1}$. Equation IV−3 can be rewritten as follows.

$$C^{-1} = M_{ss}^{-1} + H^T R^{-1} H$$
$$M_{ss} = FCF^T + \Gamma W_d \Gamma^T$$

Equation IV−4 Rewrite Equation IV−3 in steady state

The time update equation below Equation IV−4 is substituted into the above measurement update equation. When Γ is identity matrix, it is summarized for W_d as follows.

$$W_d = \left(C^{-1} - H^T R^{-1} H\right)^{-1} - FCF^T = ftn(R,C)$$

Equation IV−5 Method to calculate process covariance matrix

That is, the W_d can be expressed as a function of matrix R

and matrix C. However, in the above tuning method, the matrix W_d is created in case of only using the Kalman filter. In this paper, since the LQG controller to which the LQR controller is coupled is used, the lower error level corresponding to the matrix C is created. Therefore, W_d calculated by Equation IV-5 is set to initial value. The final W_d is determined through little tuning process.

Based on the above tuning method, the final tuning values used for scalar tracking loop and vector tracking loop are summarized in the following table. The matrix R required for calculation of the matrix W_d is based on 45 dB*Hz. The matrix R varies based on C/N0, so it is omitted in the table.

LQG-STL	$W_d = diag(1.60e-3,\ 9.99e-9, 1.11e-4)$ $\left(C = diag(1^2,\ 0.0001^2,\ 0.1^2)\right)$
LQG-VTL	$W_{d,VTL} = H_{w,k}^{\dagger} W_d (H_{w,k}^{\dagger})^T$

Table IV-3 Kalman filter process covariance matrix

The process noise covariance matrix of LQG-VTL can be calculated by using that of LQG-STL.

2. Simulation Order

Firstly, in order to check the performance of the LQG-STL, measurements estimation errors are analyzed while the movement of user changes such as static user, constant velocity, and circular movement. Comparison of the results is done for LF-STL.

Secondly, in order to investigate the performance of LQG-VTL, conditions are added one by one with the simplest simulation. Start to the simulation where only pseudorange measurement and position state are used, Doppler and velocity is added to measurement and state. To the next step, the carrier phase is added to measurement and clock bias to state. By these simulation, we can examine how the conditions are influenced in the simulation results. The above process verifies performance improvements of measurements compared to LQG-STL. In addition, while the number of satellites increase, the performance improvement of state and measurement is verified.

Finally, LQG-VTL shows robustness compared to LF-STL in temporal signal power reduction.

The above simulation procedure is summarized in the table below.

		Measurements	State	User's dynamic	C/N0 (dB*Hz)
LQG-STL	①	$\rho, \phi, \dot{\phi}$	$\rho, \phi, \dot{\phi}$	Static / Const.Vel / Circular	45
LQG-VTL	②	ρ	x, y	Static	45
	③	$\rho, \dot{\phi}$	$x, y, \dot{x}, \dot{y}$	Static	45
	④	$\rho, \dot{\phi}$	$x, y, \dot{x}, \dot{y}, B, \dot{B}$	Static	45
	⑤	$\rho, \phi, \dot{\phi}$	$x, y, \dot{x}, \dot{y}, B, \dot{B}$	Static	45
	⑥	$\rho, \dot{\phi}$	$x, y, \dot{x}, \dot{y}, B, \dot{B}$	Static	45 → 30 → 45

Table IV-4 Simulation procedure

3. Measurement Estimation Error of LQG-STL

First, the performance of LQG-STL is verified. The conditions are summarized once again as shown in the table below.

Input Variable	
Dimension	2D
Measurements	$\rho, \phi, \dot{\phi}$
State	$\rho, \phi, \dot{\phi}$
User's position	Static / Const.Vel / Circular
C/N0	35~50dB*Hz

Table IV-5 Simulation condition of LQG-STL

In the simulation results below, the solid blue line is a line showing the theoretical measurements estimation errors of LF-STL by C/N0 referenced in [6] for comparison with the result of LF-STL implemented in the simulation. The red and green lines are the standard deviation (STD) and root mean square (RMS) value of the LF-STL implemented in the simulation. The lines expressed in the purple and dark blue are the STD and RMS value of LQG-STL. The bandwidth of the loop filter is 5 Hz, and 20 Hz in case of DLL and PLL respectively.

First, the simulation results of measurements estimation errors of the static user are as follows.

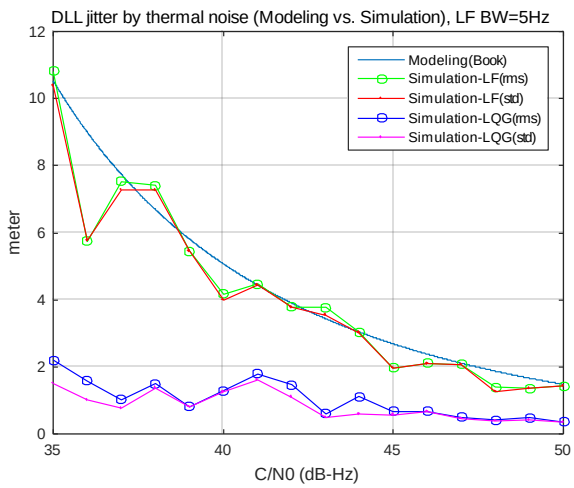

Figure IV-2 LQG-STL, Pseudorange estimation error (Static user)

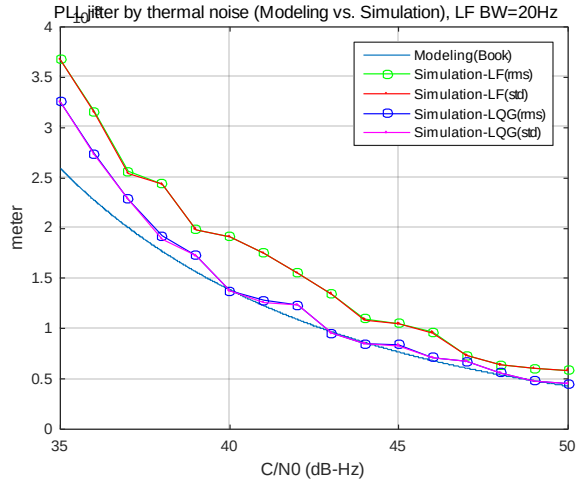

Figure IV-3 LQG-STL, Carrier phase estimation error (Static user)

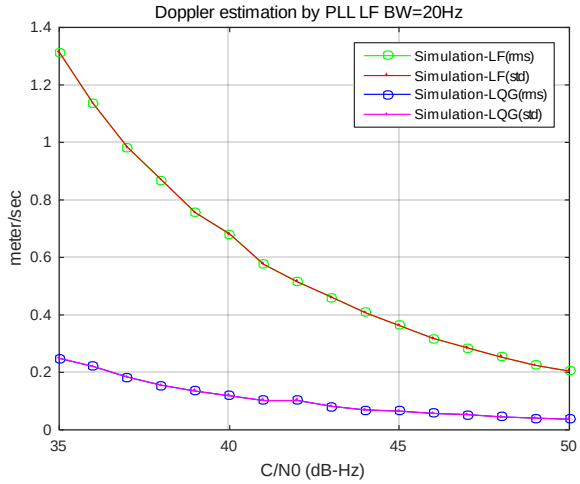

Figure IV-4 LQG-STL, Doppler estimation error (Static user)

The results of the pseudorange and carrier phase show that the theoretical calculated value of the book and the estimated

errors of the LF-STL calculated by the simulation are similar to each other. Especially, the estimation errors of LQG-STL are superior to that of LF-STL at low C/N0 value. It can be confirmed that the pseudorange is about 81% and the Doppler is about 84% reduced by 35 dB*Hz.

Next, the simulation results for the constant velocity user and the circular motion user are as follows. The velocity of the constant velocity user is 30 m/s, the radius of the circular motion is 10 m, and the angular velocity is 0.3 rad/s.

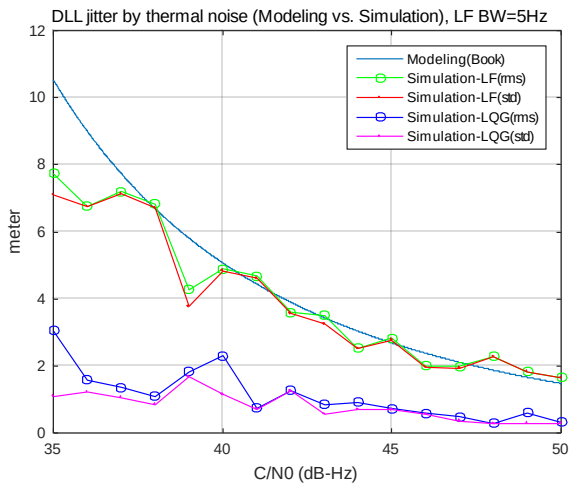

Figure IV-5 LQG-STL, Pseudorange estimation error (Const.vel user)

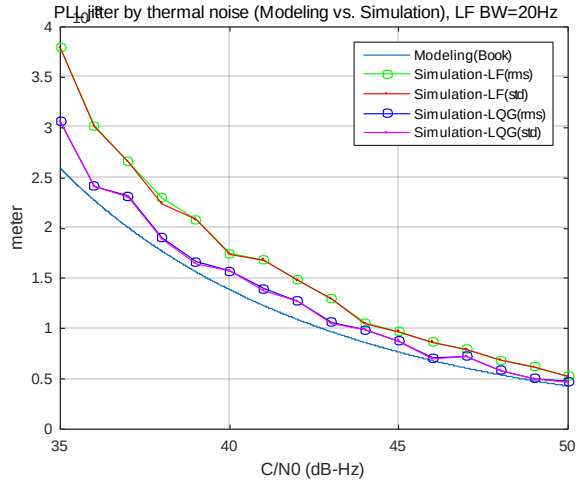

Figure IV-6 LQG-STL, Carrier phase estimation error (Const.vel user)

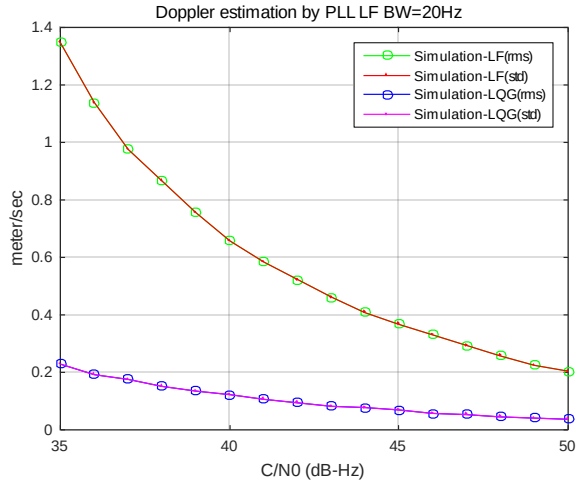

Figure IV-7 LQG-STL, Doppler estimation error (Const.vel user)

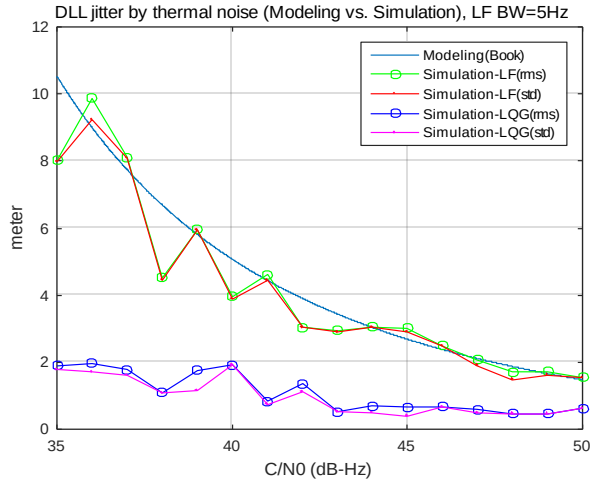

Figure IV-8 LQG-STL, Pseudorange estimation error (Circular user)

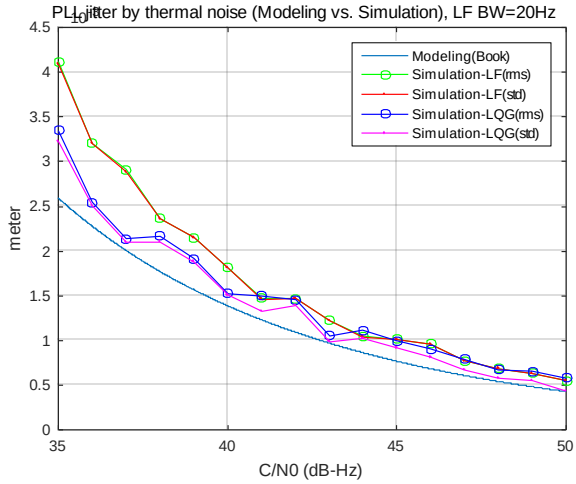

Figure IV-9 LQG-STL, Carrier phase estimation error (Circular user)

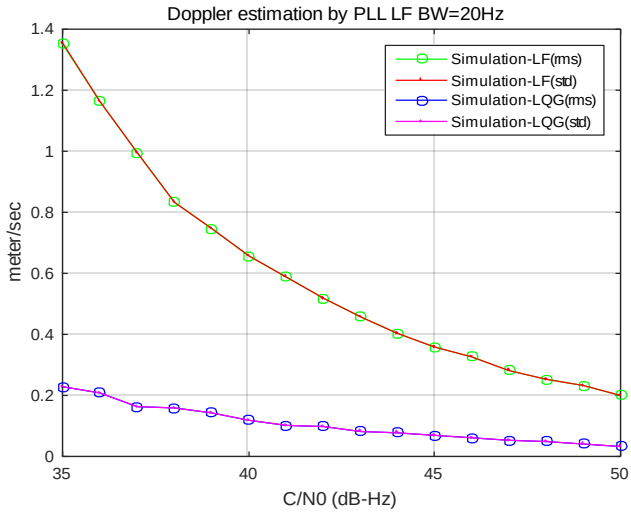

Figure IV-10 LQG-STL, Doppler estimation error (Circular user)

The same results as the static user can be confirmed even for the constant velocity user and the circular motion user. In both cases, the pseudorange estimation error of LQG-STL is about 63% and the Doppler is 84% less than that of LF-STL based on 35 dB*Hz.

Comparing the results of the carrier phase in all simulations, the performance improvement of LQG-STL compared to LF-STL is not outstanding. This is because the LQG tuning is tuned to the carrier phase level of the LF-STL. The order of the loop filter is designed as the third PLL and the second DLL, so that the PLL can keep up with the acceleration input. On the order

hand, LQG modeling is designed only up to Doppler domain corresponding to the speed. Therefore, when the user has acceleration such as circular motion user, the performance improvement of the LQG is not remarkable as compared with the LF. In addition, the performance of LQG should not be inferior to the LF in various user's motions. Therefore, the carrier phase estimation error of LQG is similar to that of the loop filter even in the case of the static user or the constant velocity user having no acceleration. These limitations can be overcome by considering the acceleration term in LQG modeling.

From the above results, it is confirmed that LQG-STL improves the estimation errors regardless of user's motion compared to LF-STL.

4. Position/Measurement Estimation Error of LQG-VTL

In section 3, we compare the LQG-STL with the LF-STL. This section verifies the improvement of the measurements errors performance of LQG-VTL versus LQG-STL. In addition, the performance of VTL according to the number of satellites is confirmed. Finally, the robustness of LQG-VTL is confirmed

compared to LF-STL in temporal signal block. This verifies robust signal tracking and additional performance improvement of position and measurements error through VTL.

All simulations are two-dimension, and the user is static. The C/N0 value is fixed at 45 dB*Hz except for the simulation of the last temporal signal attenuation situation.

(1) Measurement : ρ, State : x, y

The simplest simulation that can be implemented is a two-dimensional environment, and since there is no clock error, navigation solution can be computed by using two satellites. Simulation is carried out with increasing the number of satellites from two to five.

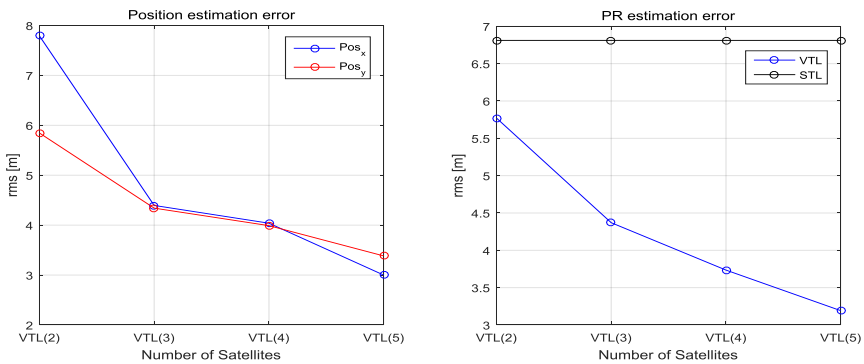

Figure IV-11 LQG-VTL (1), Position and measurement estimation errors

In Figure IV-11, the x-axis is the number of satellites and the y-axis is the RMS value of the position/measurement estimation error. In the position estimation error graph, the blue line and the red line represent the position error in the x and y directions, respectively. In the measurement estimation error graph, the black line represents the measurement estimation error of the LQG-STL and the STL is a straight line because there is no change according to the number of satellites. The blue line is the measurement estimation error of LQG-VTL.

As the number of satellites increase, the performance of the position and measurement estimation error improves to about 40%~60%, and the measurement estimation error in VTL is reduced by 53% compared with STL. The table below summarizes the following.

	State Estimation Errors		Measurement Estimation Error
	Pos_x	Pos_y	PR
VTL(2) vs. VTL(5)	62% ↓	42% ↓	45% ↓
LQG-STL vs. VTL(5)	.	.	53% ↓

Table IV-6 LQG-VTL (1), State/measurement estimation errors

(2) Measurements : $\rho, \dot{\phi}$, State : $x, y, \dot{x}, \dot{y}$

Simulation is performed by adding speed terms to the measurement and state in previous simulation. Simulation is carried out with increasing the number of satellites from two to five.

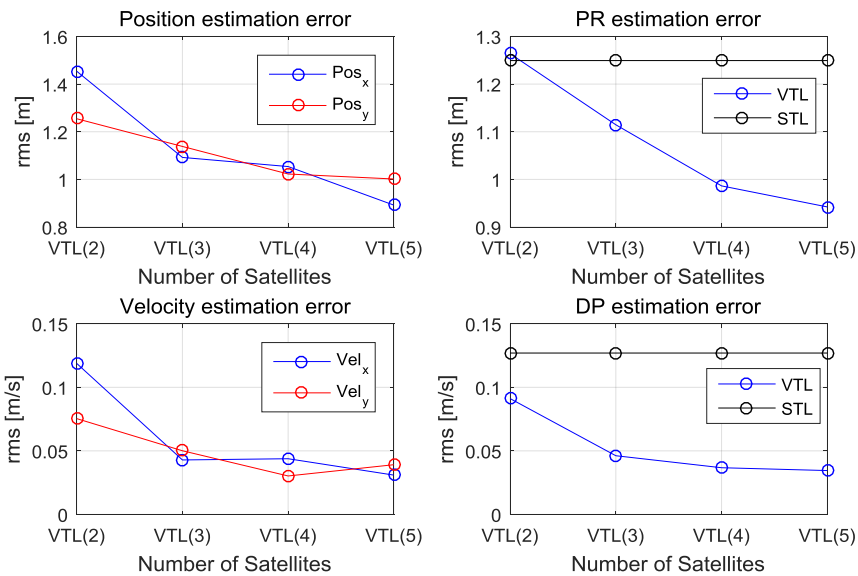

Figure IV-12 LQG-VTL (2), Position/velocity and measurements estimation errors

Figure IV-12 shows the same graph as Figure IV-11, with

user velocity and Doppler tracking error graph added. As the number of satellites increases, the position error decreases about 20~40%, the velocity error about 50~70%, the pseudorange error about 25%, and Doppler about 60. In comparison with the LQG-STL results, the measurements estimation errors are reduced by 25% in the pseudorange, and 72% in the Doppler. The table below summarizes them.

	State Estimation Errors				Measurements Estimation Errors	
	Pos_x	Pos_y	Vel_x	Vel_y	PR	DP
VTL(2) vs. VTL(5)	39% ↓	20% ↓	74% ↓	48% ↓	25% ↓	62% ↓
LQG-STL vs. VTL(5)	.	.	.	.	25% ↓	72% ↓

Table IV-7 LQG-VTL (2), State/measurements estimation errors

(3) Measurements : $\rho, \dot{\phi}$, State : $x, y, \dot{x}, \dot{y}, B, \dot{B}$

Simulation is performed by adding the clock bias and clock drift to the state in previous simulation. As the clock error is added, it is possible to calculate the navigation from three or more satellites. The number of satellites increase from three to five. The comparison is made with the result when there is no

clock error in simulation (2).

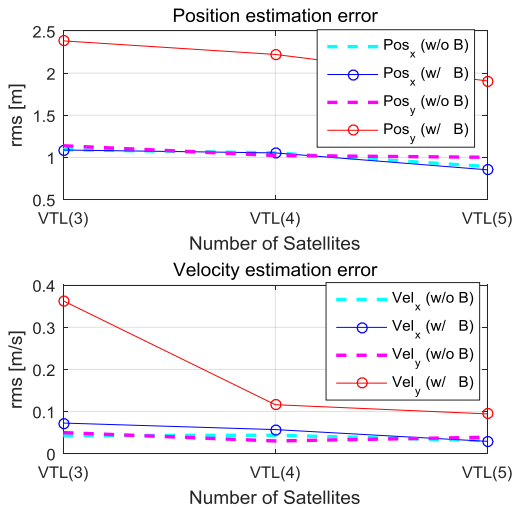

Figure IV-13 LQG-VTL (3), Position/velocity estimation errors

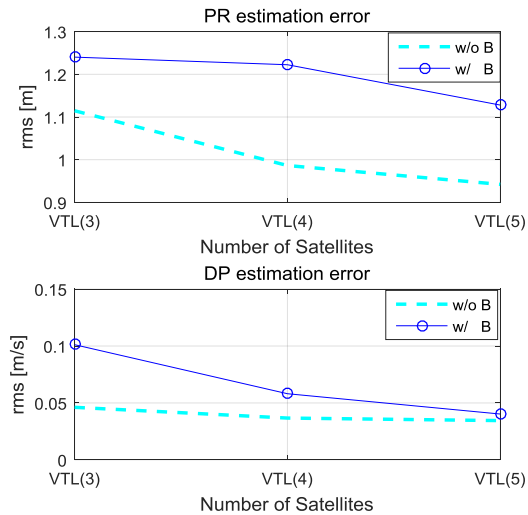

Figure IV-14 LQG-VTL (3), Measurements estimation errors

The solid line portion of the graph shows the result when there is a clock error, and the portion represented by the dotted line is the result when there is no clock error. In Figure IV-13, we can see that position/velocity estimation errors increase especially in the y direction as the clock error is added. This is because the position/velocity estimation errors are affected by the arrangement of satellites as the clock error is added. As shown in Figure IV-1, the position/velocity estimation error in the y-axis direction increases because the arrangement of satellites is in the +y direction. Figure IV-14 shows that the measurements estimation errors increase as the clock error is added. However, considering the estimation errors of velocity and Doppler, it can be confirmed that as the number of satellites increases, the error increment due to addition of clock bias decreases.

(4) Measurements : $\rho, \phi, \dot{\phi}$, State : $x, y, \dot{x}, \dot{y}, B, \dot{B}$

Simulation is performed on the assumptions that the carrier phase is added to the measurements and integer ambiguity is not considered. Simulation is carried out with increasing the number of satellites from three to six.

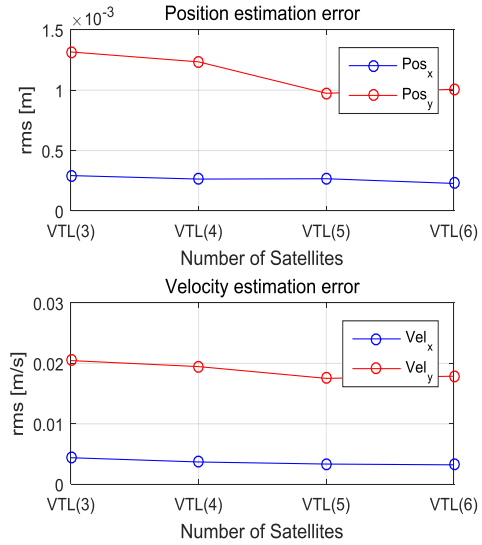

Figure IV-15 LQG-VTL (4), Position/velocity estimation errors

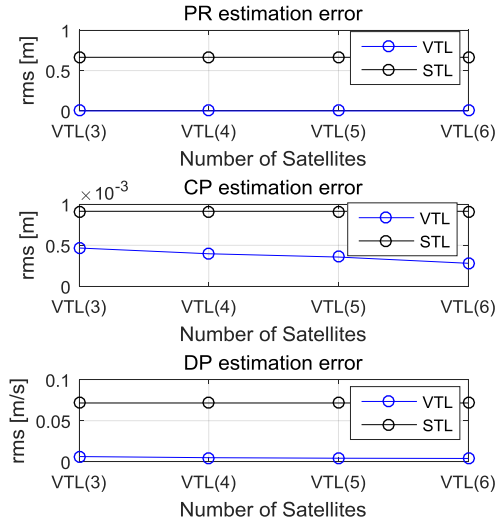

Figure IV-16 LQG-VTL (4), Measurements estimation errors

Figure IV-15, Figure IV-16 show the same graph as Figure IV-12, and the carrier phase estimation graph is added. As the number of satellites increases, the position estimation error decreases about 20%, the velocity estimation error about 10~30%, and the measurements estimation errors about 40%. Compared with the LQG-STL results, the pseudorange decreases about 99%, the carrier phase about 69% and Doppler about 94%. The table below summarizes them.

	State Estimation Errors				Measurements Estimation Errors		
	Pos_x	Pos_y	Vel_x	Vel_y	PR	CP	DP
VTL(3) vs. VTL(6)	22% ↓	23% ↓	27% ↓	13% ↓	40% ↓	40% ↓	36% ↓
LQG-STL vs. VTL(6)	.	.	.	.	99% ↓	69% ↓	94% ↓

Table IV-8 LQG-VTL (4), State/measurements estimation errors

As the carrier phase is added, it can be seen that the measurements estimation errors are significantly reduced compared to LQG-STL. The reason is that the VTL calculates the navigation solution through the Kalman filter and then estimates the measurements. The carrier phase information is used to estimate the highly accurate navigation solution. The pseudorange and carrier phase estimation are performed through

the navigation result and the line of sight vector matrix H. Since the H matrix components of the pseudorange and the carrier phase are the same, the pseudorange estimation is estimated to be similar to the carrier phase. In summary, the pseudorange is also estimated using the more accurate information, carrier phase, so that the measurements estimation errors are greatly reduced.

(5) Temporal Signal Power Reduction

This simulation is a simulation to examine the robustness of LQG-VTL. The scenario is as follows. All signal power are maintained at 45dB&Hz, but signal power is reduced to 30 dB*Hz only for one satellite after three seconds. After seven seconds, the signal power is restored to 45 dB*Hz. The current simulation tool is based on an integration time of 1ms. In the 1ms integration time environment, the signal power below 30 dB*Hz is lower than that of the noise. In other words, in order to properly receive signals below 30 dB*Hz, the integration time must be increased to amplify the signal power. In this paper, we focus on the improvement of robustness through VTL by fixing the integration time to 1ms. The simulation conditions are summarized as follows.

Input Variable	
Dimension	2D
Measurements	$\rho, \dot{\phi}$
State	$x, y, \dot{x}, \dot{y}, B, \dot{B}$
User's position	Static
C/N0	45dB*Hz (default) 30dB*Hz (3~7sec)
Satellite Number	4

Table IV-9 Simulation condition of LQG-VTL (5)

Pseudorange and Doppler are used as the measurements, and the position, velocity and clock bias are used as the state. Carrier phase is excluded from the measurement because of the integer ambiguity problem. The user location is fixed and the number of satellites is four. The signal power graph and the measurements estimation errors are shown only for second satellite where the signal attenuation occurs.

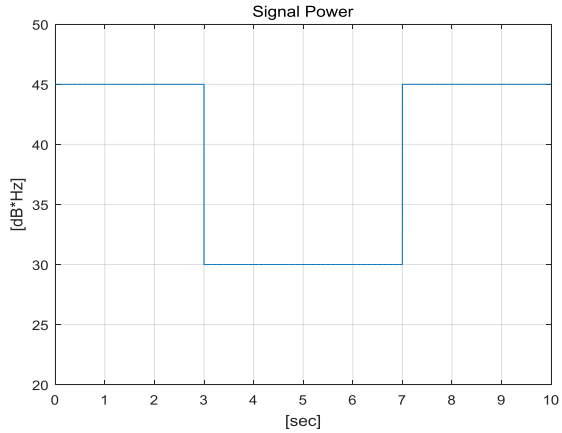

Figure IV-17 LQG-VTL(5), Signal power

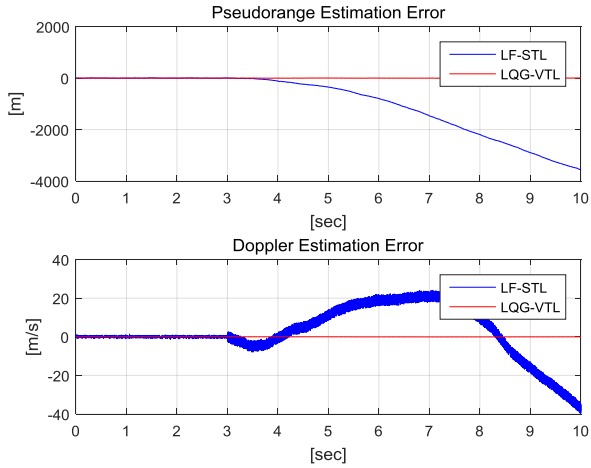

Figure IV-18 LQG-VTL (5), Measurements estimation errors

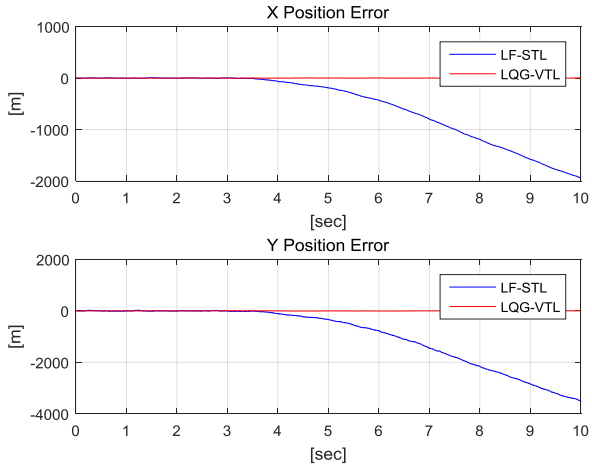

Figure IV-19 LQG-VTL (5), Position estimation error

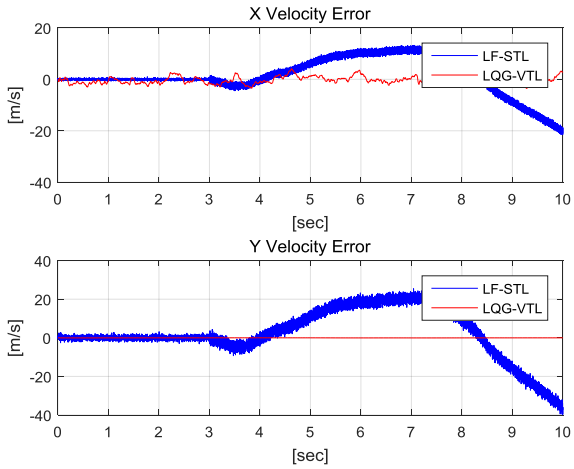

Figure IV-20 LQG-VTL (5), Velocity estimation error

After three seconds of signal power reduction, it can be seen that measurements, position, and velocity estimation errors of the LF-STL diverge. Even if the signal power is restored after

seven seconds, since the signal already loses the lock, the measurements cannot be estimated correctly. In contrast, the LQG-VTL adds a high level of measurement error of the satellite in which the signal power reduction occurs, so that it does not significantly affect the navigation solution when estimation the position through the Kalman filter. Since the estimation of the measurements is continuously and the measurements errors can be kept close to zero in the without considering various error factors. Even in the signal attenuation situation, the measurements errors are kept close to zero, the signal can be tracked immediately when the signal is restored without losing the lock.

V. Conclusion

In this paper, a study to improve the performance of the signal tracking loop of the GNSS receiver is performed. In order to improve the accuracy of the measurements, NCO inputs estimation method through the LQG controller is used instead of the conventional loop filter. In addition, VTL, which is robust to signal cutoff or attenuation, is used instead of the conventional STL. In conclusion, the necessity of LQG-VTL is verified.

In order to analyze the performance of LQG-VTL, a simulation tool is developed. In various environments and conditions, the simulations are implemented. In order to analyze the performance of the LQG controller, we compare the measurements estimation errors of LQG-STL with those of LF-STL. Simulation results show that the performance of the LQG-STL improves the pseudorange of about 60% and Doppler about 80% at 35 dB*Hz compared to the LF-STL.

Next, the simulation of the LQG-VTL is implemented by using the simplest pseudorange measurement and position state. Starting from above simulation, various simulations are performed by adding Doppler and carrier phase in measurements, and velocity and clock bias in state. In general, the position and

measurements errors performance improve with increasing number of visible satellites. In addition, the performance improvement compared to LQG-STL is confirmed. Especially, when the carrier phase is added to the measurements, it is confirmed that the accuracy of the position and measurements are greatly improved. Finally, in order to verify the robustness of the LQG-VTL, the simulation in case of temporal signal power reduction for four seconds is implemented. The LQG-VTL maintains the lock while LF-STL loses the lock. It is also confirmed that it is possible to track the signal immediately after signal recovery.

Based on the simulation results, the position and measurements performance of the LQG-VTL are analyzed. Through the developed simulation tool, it is expected that fast performance analysis will be possible before applying the LQG-VTL to the GNSS receiver in the future.

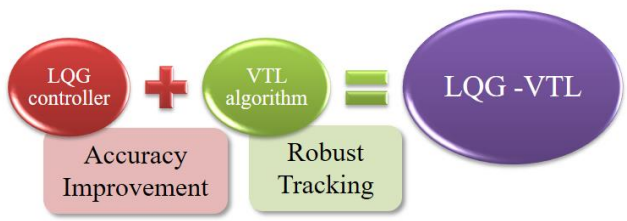

Figure V-1 Advantage of LQG-VTL

Reference

[1] B. W. Parkinson and J. J. Spilker Jr., Global Positioning System : Theory and Applications Volume □, AIAA, 1996.

[2] B. W. Parkinson and J. J. Spilker Jr., Global Positioning System : Theory and Applications Volume □, AIAA, 1996.

[3] R. M. Alkan, H. Karaman and M. Sahin, "GPS, GALILEO and GLONASS Satellite Navigation Systems & GPS Modernization," in *RAST 2005.*, 2005.

[4] M. Shaw and K. Sandhoo, "Modernization of the Global Positioning System," *GPS World Magazine,* September 2000.

[5] IS-GPS-200E, 2010.

[6] E. D. Kaplan and C. J. Hegarty, Understanding GPS Principles and Applications, ARTECH HOUSE, 2006.

[7] P. W. Ward, "Performance Comparisons Between FLL, PLL and a Novel FLL-Assisted-PLL Carrier Tracking Loop Under RF Interference Conditions," *Proceedings of the 11th International Technical Meeting of the Satellite Division of The Institute of Navigation (ION GPS 1998),* pp. 783-795, September 1998.

[8] A. M. Kamel, "Design and Testing of an Intelligent GPS Tracking Loop for Noise Reduction and High Dynamics Applications," in *ION GNSS 2010*, Portland, 2010.

[9] D. -J. Jwo, "Optimisation and sensitivity analysis of GPS receiver tracking loops in dynamic environments," *IEE Proceedings-Radar, Sonar and Navigation, Vol. 148,* pp. 241-250, August 2001.

[10] G.-I. Jee, S.-H. Im and B.-H. Lee, "Optimal Code and

Carrier Tracking Loop Design for Galileo BOC(1,1)," in *ION GNSS 20th International Technical Meeting of the Satellite Division*, 2007.

[11] S.-H. Im, J.-H. Song, G.-I. Jee and C.-G. Park, "Comparison of GPS Tracking Loop Performance in High Dynamic Condition with Nonlinear Filtering Techniques," in *ION GNSS 21st. International Technical Meeting of the Satellite Division*, 2008.

[12] S. Jeon, C. Kim, G. Kim, O. Kim and C. Kee, "Optimal Signal Tracking Algorithm for GNSS Signal using Moving Set-point LQG System," *International Journal of Control, Automation, and Systems,* vol. 11, no. 6, pp. 1214-1222, 2013.

[13] 김종원, "GNSS 수신기 신호 추적 루프 모델링과 LQG 기반 벡터 신호 추적 알고리즘에 관한 연구," 국내박사학위논문, 서울대학교 대학원, 2016.

[14] E. M. Copps, G. J. Geier, W. C. Fidler and P. A. Grundy, "Optimal Processing of GPS Signals," *Navigation Journal of the Institute of Navigation,* vol. 27, no. 3, pp. 171-182, 1980.

[15] J. J. Spilker Jr., "Vector Delay Lock Loop Processing of Radiolocation Transmitter Signals". United States Patent 5,398,034, 14 March 1995.

[16] M. Lashley, "Modeling and Performance Analysis of GPS Vector Tracking Algorithms," in *Doctor of Philosophy*, Auburn University, Auburn, Alabama, 2009.

[17] M. Lashley and D. M. Bevly, "Analysis of Discriminator Based Vector Tracking Algorithms," in *ION NTM 2007*, San Diego, CA, 2007.

[18] M. Lashley, D. M. Bevly and J. Y. Hung, "Performance Analysis of Vector Tracking Algorithms for Weak GPS Signals

in High Dynamics," *IEEE Journal of Selected Topics in Signal Processing,* vol. 3, pp. 661-673, 2009.

[19] 소형민, "의사위성 항법 시스템에서의 Vector tracking loop 수신기 구현에 관한 연구," 국내박사학위논문, 서울대학교 대학원, 2009.

[20] 전상훈, "Vector Tracking Loop를 활용한 저궤도 위성용 GPS/Galileo 소프트웨어 수신기 구현에 관한 연구," 국내박사학위논문, 서울대학교 대학원, 2012.

[21] P. Misra and P. Enge, Global Positioning System - Signals, Measurements, and Performance, Ganga-Jamuna Press, 2006.

[22] P. H. Dana, "Global Positioning System Overview," 24 12 1994. [Online]. Available: http://www.colorado.edu/geography/gcraft/notes/gps/gps.html. [Accessed 26 11 2016].

[23] G. F. Franklin, J. D. Powell and A. Emami-Naeini, Feedback Control of Dynamic Systems 6th edition, PEARSON, 2010.

[24] J. P. Hespanha, "LQR/LQG controller design," Lecture Notes, University of California, Santa Barbara, California, 2007.

[25] J. P. Hespanha, "Lecture notes on LQR/LQG controller design," Lecture Notes, University of California, Santa Barbara, California, 2005.

[26] A. E. Bryson, JR, Control of Spacecraft and Aircraft, Princeton University Press, 1994.

[27] R. G. Brown and P. Y. Hwang, Introduction to Random Signals and Applied Kalman Filtering, 4th edition, John Wiley & Sons, 2012.

[28] Y. Bulut and O. Bayat, "Kalman Filtering with Model Uncertainties," in *Proceedings of the IMAC-XXX*, Jacksonville, Florida, USA, 2012.

[29] Y. Bulut, D. Vines-Cavanaugh and D. Bernal, "Process and Measurement Noise Estimation for Kalman Filtering," in *Proceedings of the IMAC_XXVIII*, Jacksonville, Florida, USA, 2010.

[30] G. Gede, "Introduction to Kalman Filtering – An Engineer's Perspective," 20, January, 2011.

[31] V. A. Bavdekar, A. P. Deshpande and S. C. Patwardhan, "Identification of process and measurement noise covariance for state and parameter estimation using extended Kalman filter," *Journal of Process Control,* vol. 21, pp. 585-601, 2011.

초 록

GNSS를 통한 항법이 활성화 되면서, GNSS의 성능 향상을 위한 많은 연구가 진행되고 있다. 수신기 관점에서는 수신기에서 추정하는 위치와 측정치의 정확도를 높이고, 순간적인 신호 단절, 감쇠에도 신호 추적이 가능한 강건한 신호 추적 루프를 설계함으로써 GNSS 성능 향상을 이룰 수 있다. 위치와 측정치의 정확도를 높이기 위한 연구로 기존의 루프 필터를 통해 NCO 입력을 추정하는 방법 대신, 다양한 추정 이론과 제어 관점의 연구를 통해 NCO 입력을 추정하는 방법이 시도되었다. 그리고 추정 이론과 제어 이론이 결합된 LQG 제어기를 통해 NCO 입력을 추정함으로써 특정 성능 지수 조건에서 최적화된 NCO 입력을 생성하는 연구가 이루어진 바 있다. 또한 강건한 신호 추적 루프를 설계하기 위해, 기존의 스칼라 신호 추적 루프에서 벗어난 벡터 신호 추적 루프에 관한 연구가 이루어졌다. 그리고 위의 두 방법이 결합된 LQG 기반 벡터 신호 추적 루프에 관한 연구가 이루어졌으며, 이를 통해 위치, 측정치 정확도를 향상시키고 신호 방해 조건에도 강건한 신호 추적 루프를 설계할 수 있었다.

본 논문에서는 LQG 기반 신호 추적 루프를 시뮬레이션으로 구현하여, LQG 기반 신호 추적 루프의 성능을 다양한 조건에서 검증해보았다. 먼저 LQG 제어기의 성능을 검증하기 위하여 LQG 기반 스칼라 신호 추적 루프를 구성하여, 기존의 루프 필터 기반의 스칼라 신호 추적 루프와의 측정치 오차 성능을 비교하였다. 그

결과, 다양한 사용자 운동 조건에서 특히 의사거리와 도플러의 측정치 정밀도가 크게 향상됨을 확인하였다.

다음으로는 LQG 기반 벡터 신호 추적 루프를 구성하여, LQG 기반 스칼라 신호 추적 루프 대비 성능 향상을 비교하였다. 의사거리와 위치만을 측정치와 상태 변수로 가지는 단순한 시뮬레이션에서 시작하여, 측정치와 상태 변수를 증가시켜 최종적으로 의사거리, 반송파 위상, 도플러 값을 측정치로, 위치, 속도, 수신기 시계 오차, 수신기 시계 오차 변화량을 상태 변수로 갖는 시뮬레이션까지 진행하였다. 시뮬레이션 결과 벡터 신호 추적 루프에서 신호 추적이 가능한 위성 개수가 증가할수록 사용자 위치, 측정치 성능이 향상됨을 확인하였고, LQG 기반 스칼라 신호 추적 루프 대비 측정치 성능 향상 또한 확인하였다. 또한 반송파 위상이 측정치로 추가되면, 위치와 측정치 정확도가 크게 향상되는 것을 확인하였다. 마지막으로 순간적인 신호 감쇠 상황에서, 루프 필터 기반 스칼라 신호 추적 루프와의 비교를 통해 신호 추적의 강건성을 확인하였다.

향후 GNSS 수신기에 LQG 기반 신호 추적 알고리즘을 적용하기 전, 제안된 알고리즘의 빠른 성능 평가가 가능할 것으로 기대된다.

주요어 : 신호 추적, GNSS 수신기, LQG 제어, 벡터 신호 추적, 스칼라 신호 추적, 위치 정확도, 측정치 정확도

학 번 : 2015-20769